NATIONAL AERONAUTICS AND SPACE ADMINISTRATION

Technical Report 32-1590

A Model of the Physical Properties of Comet Encke

F. W. Taylor
C. M. Michaux
R. L. Newburn, Jr.

CASE FILE
COPY

JET PROPULSION LABORATORY
CALIFORNIA INSTITUTE OF TECHNOLOGY
PASADENA, CALIFORNIA

October 1, 1973

NATIONAL AERONAUTICS AND SPACE ADMINISTRATION

Technical Report 32-1590

A Model of the Physical Properties of Comet Encke

F. W. Taylor
C. M. Michaux
R. L. Newburn, Jr.

JET PROPULSION LABORATORY
CALIFORNIA INSTITUTE OF TECHNOLOGY
PASADENA, CALIFORNIA

October 1, 1973

Preface

The work described in this report was performed by the Space Sciences Division of the Jet Propulsion Laboratory.

Comet Encke is presently regarded as the likely target of NASA's first cometary mission, probably a slow flyby projected to take place in 1980. This document presents a model of Encke which is intended to be useful for the design of scientific experiments and spacecraft systems for such a mission.

Data on the physical properties of comets are generally very sparse, and Encke is no exception. Much of the numerical information contained herein is, therefore, based on calculations of a highly conjectural nature, and the results have large uncertainties associated with them. The user is cautioned that this is a model and not a specification, and must be treated as such if it is to be useful.

The starting point for this work was an earlier study of Encke (Ref. 9) prepared by the TRW Systems Group under contract to JPL. Information from that document formed a cornerstone of the present model. The cooperation of D. M. Wexler of the Environmental Requirements Section of JPL, who made the flow calculations described in Section III-C, was greatly appreciated. D. K. Yeomans of the Computer Sciences Corporation kindly gave permission to reproduce his unpublished compilations of observational data which appear in Tables 3 and 4.

Contents

Contents (contd)

Tables

Figures

Contents (contd)

Figures (contd)

Contents (contd)

Figures (contd)

Abstract

The available observational data on periodic comet Encke have been collected and interpreted in order to construct a model of the comet. The model is intended for use in the design of scientific experiments and spacecraft systems to be used on future missions to Encke. Numerical values and ranges of uncertainty are given for all of the important structural, compositional, and photometric parameters with references to the original research from which these were calculated or estimated.

A Model of the Physical Properties of Comet Encke

I. Introducticn

Comet Encke was discovered in 1786 and has since revealed itself as a periodic object returning to perihelion approximately every 3.3 yr. The orbital elements are given in Table 1. It follows that Encke had made at least 56 passages around the Sun, and probably many more. The analysis by Whipple and Hamid (Ref. 1) of the Taurid meteor stream suggests a capture date at least 5000 yr ago. It is, therefore, a fairly old comet, and indeed it is presently showing signs of coming close to the end of its active life. Taking the nineteenth century photometric observations at face value, Encke has decreased in brightness by about 3 magnitudes in the last century. It shows greatly reduced activity after perihelion relative to before, and shows very little continuum radiation at any time, indicating a low dust content. Encke never shows a type II (dust) tail and in some apparitions has shown no tail at all. Similarly, stellar condensations presumably associated with the presence of a nucleus have been variously reported as being present or absent.

Encke was recently observed at aphelion as a star-like object of magnitude 20.5 (Ref. 2). At this time it was more than 4 AU from the Sun. A survey (Ref. 3) of observations from 1885–1951 indicates that the coma typically becomes observable at about 1.5 AU with the first appearance of the tail at about the same distance. During the last apparition Encke had an absolute visual magnitude (i.e., at 1 AU from the Sun and 1 AU from Earth) of 10.8.*

Table 1. Orbital characteristics of comet Encke

Parameter	Value
Orbital period, yr	3.30
Aphelion distance, AU	4.09
Perhelion distance, AU	0.34
Orbital inclination, deg	12.4
Velocity at 1 AU, km-s^{-1}	37.1
Velocity at perihelion, km-s^{-1}	69.9
Orbital eccentricity	0.847

II. Dimensions

The nominal and limiting values assigned to the dimensions of the nucleus, coma, and tail of Encke are shown

*IAU Circular No. 2547, and Z. Sekanina, private communication.

in Table 2. The derivation of these values is presented below.

A. Nucleus

Roemer (Ref. 4) has estimated the product $a_n R_n^2$ to be 0.24 (a_n = geometric albedo, R_n = radius of the nucleus in kilometers) from observational estimates of the magnitude of the nucleus of Encke. Thus R_n is determined as a function of the assumed albedo. The upper limit on R_n in Table 2 corresponds to $a_n = 0.02$, which is the albedo of the blackest known asteroids (Ref. 5), while the lower limit is for $a = 0.7$, which is the albedo of an ice-covered sphere.

The value of aR_n^2 itself is fairly uncertain. Marsden and Sekanina (Ref. 6) have redone Roemer's calculation for Encke assuming a different phase function, and have obtained $a_n R_n^2 = 0.32$. Maines et al. (Ref. 7) obtained the same value. Roemer's recent (Ref. 2) observation of Encke at aphelion as an object of magnitude 20.5 corresponds to $aR_n^2 = 0.8$. These variations have been considered absorbed in the larger range of uncertainty in a_n for the purposes of forming the model, which uses the value 0.32.

B. Coma

Vsekhsvyatskii (Ref. 3) has compiled 37 observations of the diameter of Encke's coma reduced to a Sun–comet distance of 1 AU (Fig. 1). The nominal value for the diameter of 10^5 km and the upper and lower limits of 2×10^4 and 2×10^5 km are derived from these statistics, which cover the apparitions from 1848 to 1964. Yeomans (Ref. 8) gives a list of 24 uncorrected observations of the coma diameter for the period 1957–1970 (Table 3) which are consistent with these limits.

Table 2. Physical dimensions of Encke model

Parameter	Low extreme	Nominal model	High extreme
Radius of nucleus, km	0.67	1.3	4
Radius of coma at 1 AU, km	10^4	5×10^4	10^5
Length of tail,[a] km	10^5[b]	10^6	3×10^6
Mass, g	1.2×10^{14}	9.2×10^{15}	8×10^{17}

[a]Measured from nucleus.

[b]Indistinguishable from nominal coma.

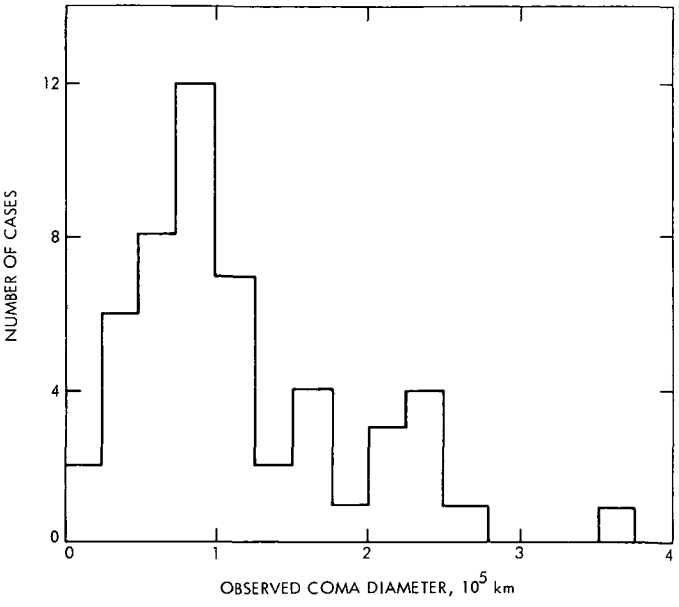

Fig. 1. Summary of observations of the diameter of Encke's coma, reduced to a distance of 1 AU (after Vsekhsvyatskii, Ref. 3)

Vsekhsvyatskii's data also permits an estimate of the variation in the diameter of the coma with heliocentric distance. The observations are plotted in Fig. 2, showing

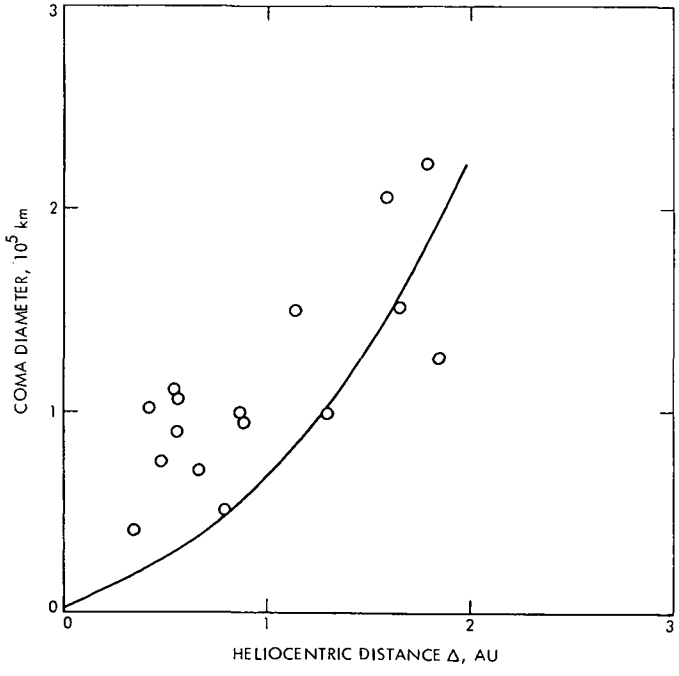

Fig. 2. Dependence of coma diameter on heliocentric distance. The curve is the theoretical law $d = a\,\Delta^{7/4}$ with $a = 0.66 \times 10^5$ km$^{-3/4}$

Table 3. Observed coma diameters for comet Encke[a]

Date	Observed angular diameter of coma, seconds of arc	Geocentric distance, AU	Linear size of coma, km	Observatory	Exposure time, min	Aperture, in.
1957 July 25	10	1.79	12,978	Lick		
28	12	1.72	14,964	Flagstaff Sta.	32	40 *f*/6.8
31	15	1.66	18,052	Lick	30	36
Aug. 24	60	1.20	52,200	McDonald	10	82
29	60	1.12	48,720	Lick	6	36
Sept. 4	42 × 60	0.92	28,014 × 40,020	Flagstaff Sta.	10	40 *f*/6.8
19	60	0.92	40,020	Flagstaff Sta.	1.5	40 *f*/6.8
28	180[b]	0.93	121,365	Yerkes	1	24
Oct. 1	180	0.96	125,280	Yerkes	0.5	24
1960 Nov. 10	36	0.89	23,229	Flagstaff Sta.	60	40
Dec. 7	10	0.89	6,452	Yerkes	10	24
13	20	0.88	12,760	Yerkes	5	24
19	60	0.87	37,845	Flagstaff Sta.	15	40
1961 Jan. 6	60	0.79	34,365	Flagstaff Sta.	15	40
6	180	0.79	103,095	Flagstaff Sta.	30	40
7	180	0.78	101,790	Flagstaff Sta.	30	40
11	180	0.75	97,875	Flagstaff Sta.	60	40
17	48	0.71	24,708	Flagstaff Sta.	0.5	40
17	180	0.71	92,655	Flagstaff Sta.	30	40
1963–1964						
1967						
1970 Oct. 21	90	0.73	47,632	R. Waterfield	80	6 *f*/4.5
Nov. 1	180	0.66	86,130	Crimean		
16	480	0.60	208,800			binoculars

[a]Reproduced from Ref. 8.

[b]This value was given as 3″ in original reference. It seems likely that the correct value was 3′ or 180 seconds of arc.

considerable scatter. A theoretical law for the heliocentric dependence may be obtained assuming that the visible diameter is proportional to the product of the expansion velocity of the gas and its photodissociation time. If the former depends on the square root of temperature, which in turn is proportional to the fourth root of the insolation, and the photodissociation time is inversely proportional to the insolation, it follows that

$$\left.\begin{aligned} D &\propto [(\Delta^{-2})^{1/4}]^{1/2} \cdot \Delta^2 = \Delta^{-1/4} \cdot \Delta^2 = \Delta^{7/4} \\ D &= a\,\Delta^{7/4} \end{aligned}\right\} \quad (1)$$

The curve obtained using a value of 0.66×10^5 km$^{-3/4}$ for the constant a is shown in Fig. 2. This corresponds to a fit to the data when the more recent observations are given more weight.

C. Tail

Figure 3 summarizes the observational material on tail length from Ref. 9 and Table 4 (Ref. 8). These data are the basis for the model values in Table 1.

D. Mass

No measurements of the mass of Encke are available. The values used in Table 2 are derived from the radius estimates assuming a nominal density of 1 g-cm^{-3}, with extreme values of 0.1 g-cm^{-3} (porous rock or snow, or some combination of both) and 3 g-cm^{-3} (silicate rock).

Table 4. Observed tail lengths for comet Encke[a]

Date	Observed angular length of tail, min of arc	Δ, AU	δ, AU	R, AU	β, deg	Tail length[b] S, AU	Tail length[b] S, km	Observatory	Exposure, min	Aperture, f-ratio, in.
1957 July 30	0.5	1.58	1.68	1.02	36.3	0.0004	59,800	Flagstaff Sta.	30	40 f/6.8
Sept. 24	2	0.71	0.93	1.01	74.7	0.0006	89,700	Yerkes	1	24
	25	0.71	0.93	1.01	74.7	0.0070	1,046,500			
28	40	0.64	0.93	1.00	76.7	0,0112	1,674,400	Yerkes	1	24
Oct. 1	65	0.59	0.96	1.00	76.2	0.0188	2,810,600	Yerkes	0.5	24
2	60	0.57	0.97	1.00	76.2	0.0175	2,616,250	Yerkes	1	24
4	65	0.53	0.99	1.00	75.6	0.0194	2,900,300	Yerkes	1	24
1961 Jan. 4	1	0.83	0.80	0.98	73.9	0.0002	29,900	Yerkes	1	24
6	7	0.80	0.79	0.98	73.9	0.0017	254,150	Flagstaff Sta.	15	40 f/6.8
7	10	0.78	0.78	0.98	77.8	0.0023	343,850	Flagstaff Sta.	30	40 f/6.8
11	20	0.71	0.75	0.98	84.3	0.0044	657,800	Flagstaff Sta.	60	40 f/6.8
17	20	0.62	0.71	0.98	94.7	0.0041	612,950	Flagstaff Sta.	30	40 f/6.8
18	120	0.62	0.71	0.98	94.7	0.0248	3,707,600	A. McClure		7 f/7
1964 Aug. 30	0.5	1.67	1.10	1.01	35.8	0.0003	44,850	Flagstaff Sta.	45	40 f/6.8
1967										
1970										

[a]Reproduced from Ref. 8.

[b]The tail length (S) has been corrected for projection effects using the formula:

$$S = \frac{\Delta \sin t}{\sin(\beta - t)}, \text{ where } \cos\beta = \frac{\delta^2 + \Delta^2 - R^2}{2r\Delta}$$

$t \equiv$ observed angular length of tail

$\delta \equiv$ geocentric distance in AU

$\beta \equiv$ phase angle (Sun-comet-Earth)

$\Delta \equiv$ heliocentric distance of comet

$R \equiv$ heliocentric distance of Earth

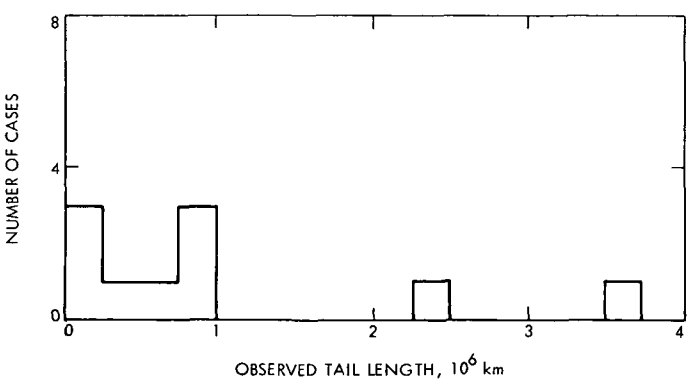

Fig. 3. Summary of observations of Encke's tail length (Ref. 9)

III. Structure and Composition

A. General

The appearance and behavior of Encke are consistent with the icy conglomerate model of Whipple (Ref. 10). The reduced activity of Encke observed following each perihelion passage, the secular decrease in the nongravitational force acting on the nucleus, and the overall decline in magnitude during successive apparitions over the last century (Refs. 11 and 12) are evidence for a nucleus consisting almost entirely of a porous, rocky core with the remaining conglomerate material (rocky fragments embedded in ice) distributed on the surface and

within the pores. A study of the nongravitational deviations in the motion of Encke (Ref. 13) supports this picture. The rocky core is probably similar to the Apollo asteroids (e.g., Icarus), which are thought by some to be defunct comets. The ice is principally H_2O, perhaps with NH_3 and CH_4 plus other molecules and radicals trapped as clathrate hydrates. These are physical compounds in which molecules of methane, for example, are held within the lattice of water ice crystals so that the rate of sublimation of all species is controlled by that of H_2O. The ratio of water molecules to trapped molecules is six to one for the clathrate hydrate of methane, and is probably the same for other clathrates (Ref. 14). The presence of clathrates rather than discrete condensates is required to explain the observed emissions of daughter species and is plausible on physiochemical grounds (Refs. 14–17). In particular, Delsemme and Wenger (Ref. 14) show that the clathrate ices are more stable than the separate forms and will, therefore, tend to be preferentially formed. The existence of the condensible phase as clathrates also implies a mechanism for the release of these compounds under solar irradiance. The laboratory experiments with the clathrate hydrate of methane of Delsemme and Wenger (Ref. 14) show that this compound dissociates by releasing gas which strips off icy grains. A halo of such grains is, therefore, expected to form within the inner coma of Encke. This is not only physically plausible, it also provides a mechanism for the observed lifetimes of the evaporated molecules and radicals released into the coma. Delsemme and Miller (Refs. 15–17) show that the observations of most comets are consistent with a single dominant lifetime (i.e., that of the grains) rather than the various lifetimes to be expected from species released individually from the nucleus.

The physical picture of Encke that emerges (Fig. 4) is of a rocky asteroidal core impregnated and partially

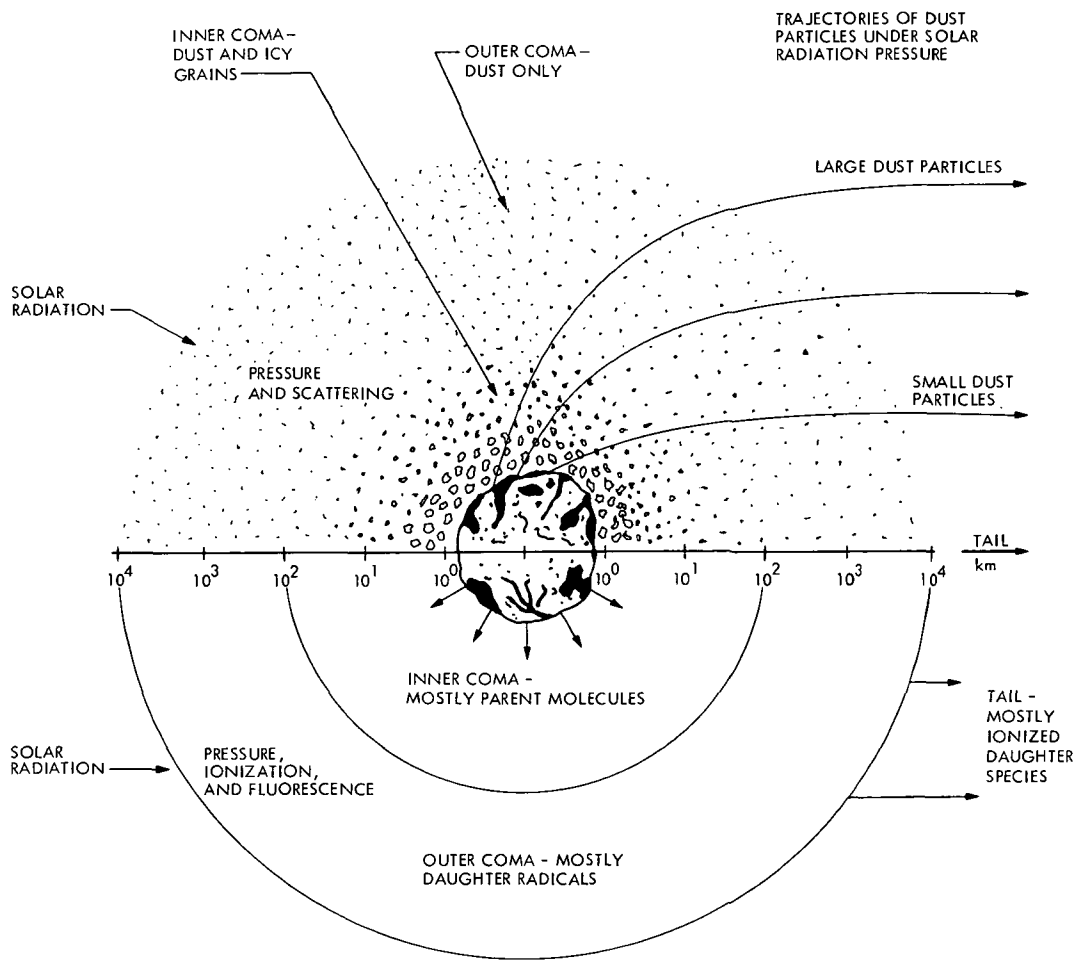

Fig. 4. Simplified schematic diagram showing structure of Encke model. The upper and lower parts represent the solid particle and gaseous structure, respectively

covered with clathrate ices which are expelled as grains with an increasing rate as the comet approaches the Sun, forming a halo around the nucleus. The gaseous atmosphere is formed by evaporation from both the nucleus and the grains in the halo.

These gases diverge from the nucleus and inner coma with thermal velocities of 400–700 m-s^{-1}. Their abundance falls off rapidly with increasing distance from the nucleus due to photodissociation to form the so-called "daughter" species. These radicals are excited by resonance fluorescence and emit the radiation which is observed visually and spectroscopically on Earth. Table 5 presents a list of the species which have been observed in Encke, and others which are seen in some comets (although not Encke) and are presumably present below the observational threshold in Encke. Section III-C describes a model of the distribution of the different species as a function of distance from the nucleus.

Rocky particles as well as condensed gases are ejected from the nucleus. The smaller particles (dust) will be partially contained within the icy grains and will be released as the grains dissociate. A model of the sizes and distribution of dust and larger solid particles is given in Section III-E. A model for the rate of impact of particles on a body such as a spacecraft which ventures inside the comet is derived from the dust model in Section III-F.

B. Composition

The composition of Encke may be inferred indirectly by considerations of the likely composition of the Taurid meteors, which have their origin as matter expelled from Encke (Refs. 18 and 19), and by interpretation of the emission spectrum. Taurid meteors have never been recovered for analysis, but the concentrations of metallic ions released into the upper atmosphere during β-Taurid showers have been measured by mass spectrometer (Ref. 20). Observations of their trails also contain some information. The trails are extremely clean and show no terminal blending, which is indicative of high tensile strength (Ref. 21). However, the deceleration rates are quite normal, showing that Taurids are not denser than average. Both sets of evidence are consistent with those stony particles known as chondrites; nearly 90% of all falls belong to this class (Ref. 22). Then the rocky core of Encke will be expected to contain the minerals common to chondrites as shown in Table 6.

The volatile component of the nucleus is likewise identifiable only indirectly because the observable species in the coma (CN, CH, NH, etc.) are probably not present in the nucleus but instead are produced in the inner coma by photodissociation of the gases emitted by the nucleus. Delsemme (Ref. 23) has described an attractively simple model in which the only volatile constituents of the nucleus are H_2O, NH_3, and CH_4 ices. These absorb solar energy to undergo dehydrogenation reactions leading to CO, CO_2, N_2, HCN, and higher hydrocarbons, which then undergo photodissociation leading to the observed radicals. However, the results of more recent

Table 5. Species observed in the spectrum of Encke (Ref. 9)

Species[a]	Wavelength, Å	Strength[b]
CN	3880	S
C_2	4740	S
	5160	
	5640	
C_3	4050	S
CH	4280	W
NH	3360	W
NH_2	6300	W
OH	3090	W
CO^+	4000	W
	4260	
	4550	
N_2^+	3910	W

[a]Other species probably present: OH^+, CH^+, Na, CO_2^+, Fe, Ni, N_2^+.

[b]S = strong; W = weak.

Table 6. Qualitative composition of Encke's nucleus

Nonvolatile component:	Olivine
	Orthopyroxene
	Kamacite
	Taenite
	Troilite
	Plagioclase feldspar
	Clinopyroxene
Volatile component:	H_2O ice
	CH_4 ice[a]
	NH_3 ice[a]

[a]Probably as the clathrate hydrate $X \cdot n\ H_2O$.

work have led Delsemme himself (Ref. 15) to suggest that a more complex model is required. Firstly, the discovery of molecules like HN_3 and CH_2O in interstellar space constitutes circumstantial evidence for the possible presence of such species in the cometary nucleus. Secondly, Jackson and Donn (Ref. 24) have pointed out that there is insufficient energy in the solar flux to provide the heating required to convert NH_3 and CH_4 into the other parent species. Finally, the lifetimes of some of the prime candidates as parent molecules are much too long to explain the observed (Refs. 25–28) production rates of radicals. This criterion seems to require that unsaturated molecules or radicals (which could provide energy through exothermic reactions) are present in the nucleus. Possibly the observed radicals are present initially and are not products of photodissociation at all.

The above brief discussion shows that the question of the volatile composition of the nucleus is completely open. About the only thing that can be said with reasonable certainty is that large amounts of water ice are present. This follows from observations of Lyman-α emission from Encke (Ref. 29), which is indicative of an extensive atomic hydrogen halo, and the accompanying presence of OH. Also, the presence of large amounts of H_2O in the nucleus is necessary for the formation of clathrate compounds, which appear to fit the observed evaporation rates quite well (Refs. 14–17). The presence of NH_3 and CH_4 is to be expected on cosmogonological grounds, whether or not they are the parents of the observed radicals. If a cosmic abundance of elements is assumed for the material from which the comet formed, then it would be expected that the C, N, and O will be fully hydrogenated before the excess H_2 and He was lost in the early history of the comet. The NH_3 and CH_4 would condense as hydrates, and the composition of the result would be (Ref. 30):

12%	CH_4
62%	CH_4 hydrate
12%	NH_3 hydrate
14%	other

In this list "other" is mainly the rocky material. In present day comet Encke, such a composition will have been modified by the loss of most of the volatiles. The observed rate of decay of the magnitude of Encke (Figs. 5 and 6) fitted to a simple law (Ref. 11) suggests a "death date" for Encke of around 2000 AD. This is consistent with Sekanina's (Refs. 13 and 31) independent estimate of 2030 AD. Converted to terms of remaining volatiles, and

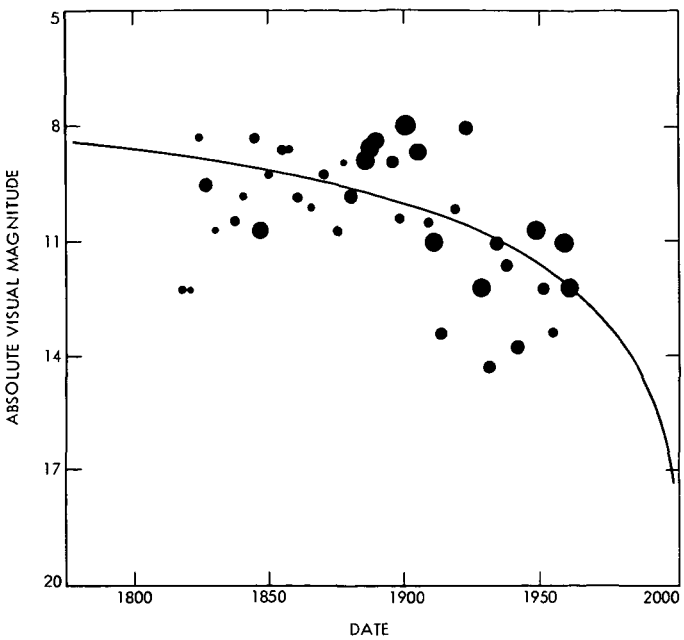

Fig. 5. Observed magnitude of Encke as a function of time from Ref. 11. The size of the point is proportional to the weight assigned to the observation. The curves are theoretical fits to the points; see text

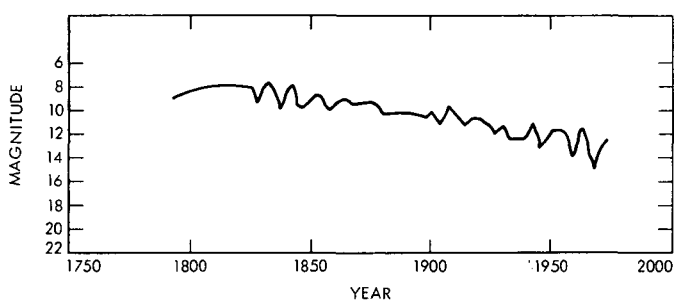

Fig. 6. Observed magnitude of Encke as a function of time from Ref. 12

assuming that all of the CH_4 is lost first, the composition of Encke in 1980 should be roughly

29%	CH_4 hydrate
5.6%	NH_3 hydrate
65.4%	other

Recalling the arguments of the previous section, the list should perhaps include substantial amounts of unsaturated molecules and radicals trapped as hydrates. The likely abundances of these cannot be estimated at the present time. If their presence, and the presence of compounds of uncommon elements, is neglected entirely and "other" is taken to refer strictly to chrondritic material, then a tentative model for the chemical composition in

Encke's nucleus can be derived (Table 7), using data from Ref. 22.

C. Density Profiles Within the Coma

Mendis et al. (Ref. 32) have performed a complete hydrodynamic analysis of a cometary atmosphere initially consisting entirely of H_2O, including frictional interaction between H_2O and its daughter products as well as production and loss mechanisms. From such calculations the radial distribution and flow velocities of H_2O and their daughter species can be determined. These quantities are plotted in Figs. 7–10 and 11–14 for heliocentric distances of 0.34, 0.8, 1.0, and 2.0 AU. In the derivation of these curves, it was assumed, following Mendis et al.,

Table 7. Model for the chemical composition of the nucleus of P/Encke

Element	Composition, %
Silicates[a]:	
SiO_2	25.0
MgO	15.6
FeO	7.8
Al_2O_3	1.8
CaO	1.2
Na_2O	0.6
K_2O	0.1
Cr_2O_3	0.2
MnO	0.2
TiO_2	0.1
P_2O_5	0.1
H_2O	0.2
Metals:	
Fe	7.6
Ni	0.9
Co	0.1
Other nonvolatiles:	
FeS	3.9
P	0.1
Volatiles:	
H_2O	27.7
CH_4[b]	4.2
NH_3[b]	2.8

[a]Oxidized elements which make up the complex silicate minerals are reported as oxides, following the convention in rock analysis.

[b]Present as the hydrate.

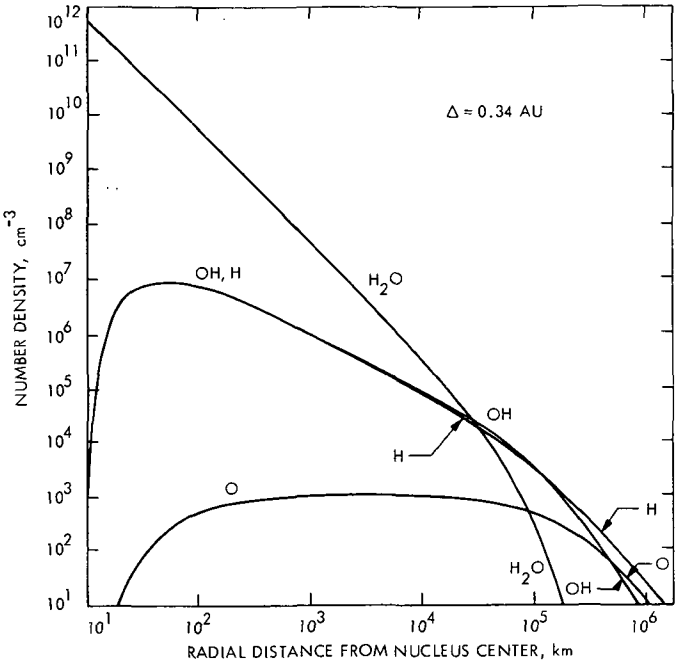

Fig. 7. Distribution of H_2O and its daughter products as a function of distance from the nucleus at perihelion. This model assumes all of the H_2O is emitted directly from the nucleus (after Ref. 32)

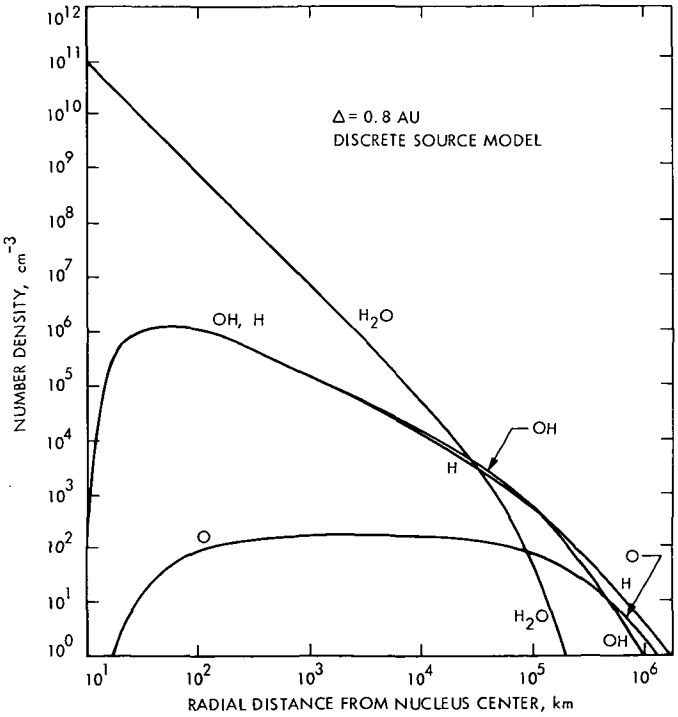

Fig. 8. Distribution of H_2O and its daughter products as a function of distance from the nucleus at a heliocentric distance of 0.8 AU (after Ref. 32)

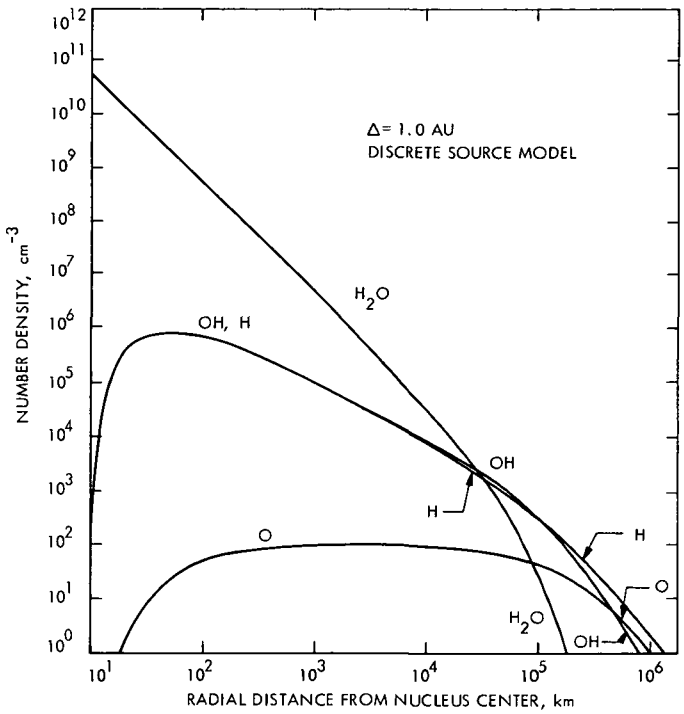

Fig. 9. Distribution of H_2O and its daughter products as a function of distance from the nucleus at a heliocentric distance of 1 AU (after Ref. 32)

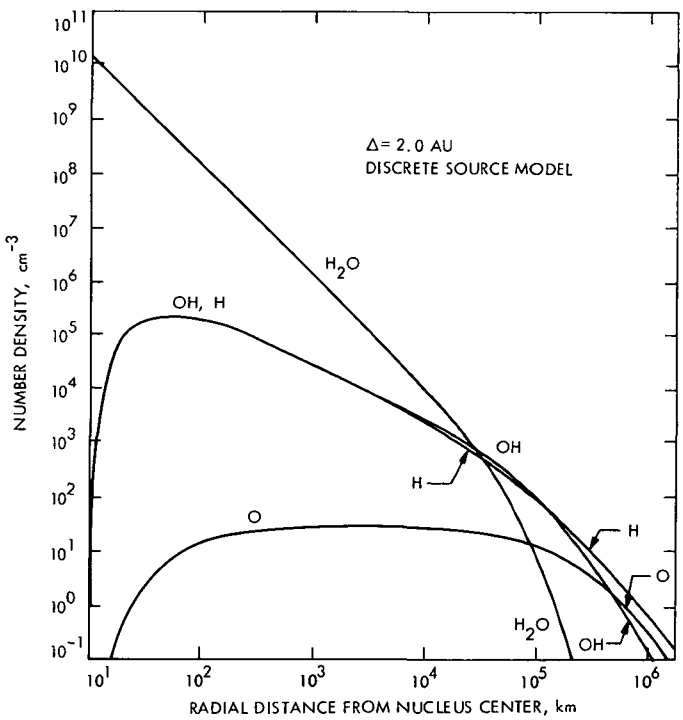

Fig. 10. Distribution of H_2O and its daughter products as a function of distance from the nucleus at a heliocentric distance of 2 AU (after Ref. 32)

that all of the H_2O is released within 10 km from the center of the nucleus ("discrete source model"), although the absolute amount was reduced by one order of magnitude from Mendis' value to be appropriate for Encke. This value is consistent with the estimated rate of ejection of H atoms of 5×10^{26} atoms-sr^{-1}-s^{-1} obtained by Bertaux et al. (Ref. 29) from observations of the Lyman-α emission of the hydrogen cloud surrounding Encke using the OGO-5 satellite. It also matches Sekanina's (Ref. 31) estimate of the rate of mass loss from Encke based on studies of the secular change in the nongravitational forces.

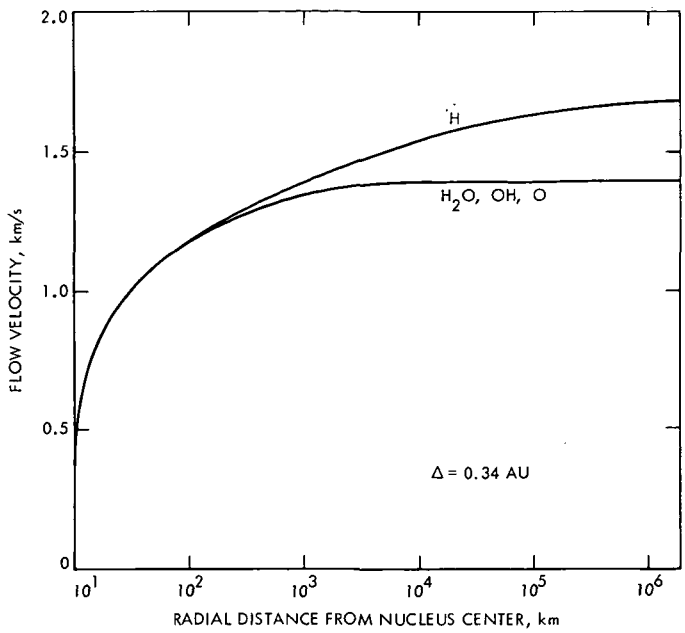

Fig. 11. Flow velocity as a function of radial distance at perihelion (after Ref. 32)

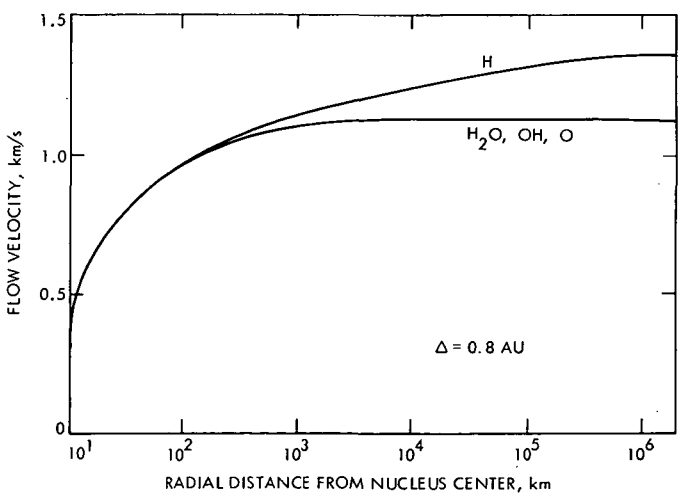

Fig. 12. Flow velocity as a function of radial distance at a heliocentric distance of 0.8 AU (after Ref. 32)

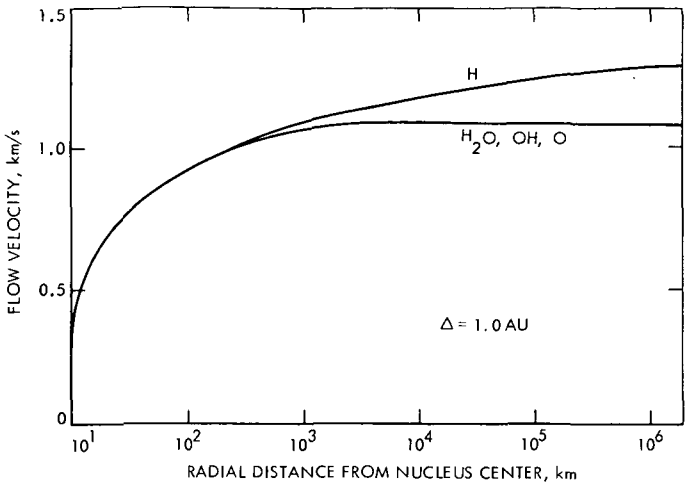

Fig. 13. Flow velocity as a function of radial distance at a heliocentric distance of 1 AU (after Ref. 32)

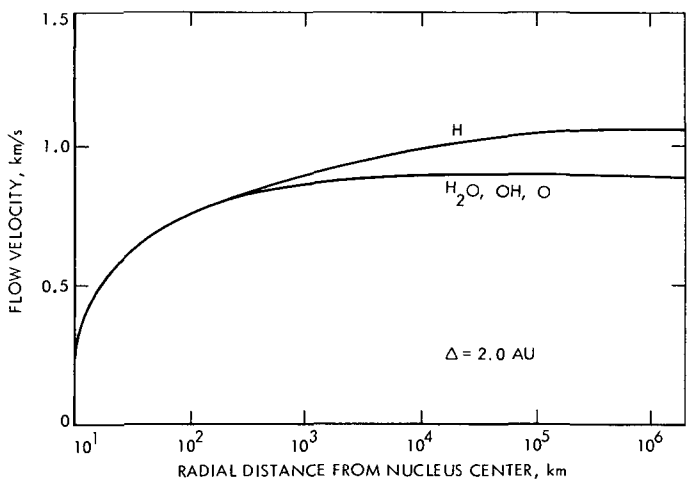

Fig. 14. Flow velocity as a function of radial distance at a heliocentric distance of 2 AU (after Ref. 32)

The discrete source model is inconsistent with the model proposed here, in that the nucleus is probably surrounded by a halo of icy grains which evaporate continuously. This forms an extended source of H_2O, perhaps 10^3 km in extent ("icy halo model"). Mendis et al.'s formulations have been modified by D. M. Wexler to take account of this effect and the density and velocity profiles recomputed. The results for the densities at 0.8 and 1.0 AU are shown in Figs. 15 and 16. The differences between these and the corresponding discrete source curves are quite small, less than a factor of 2 at most. The velocity profiles are virtually identical for the two cases, so Figs. 11 through 14 apply to both.

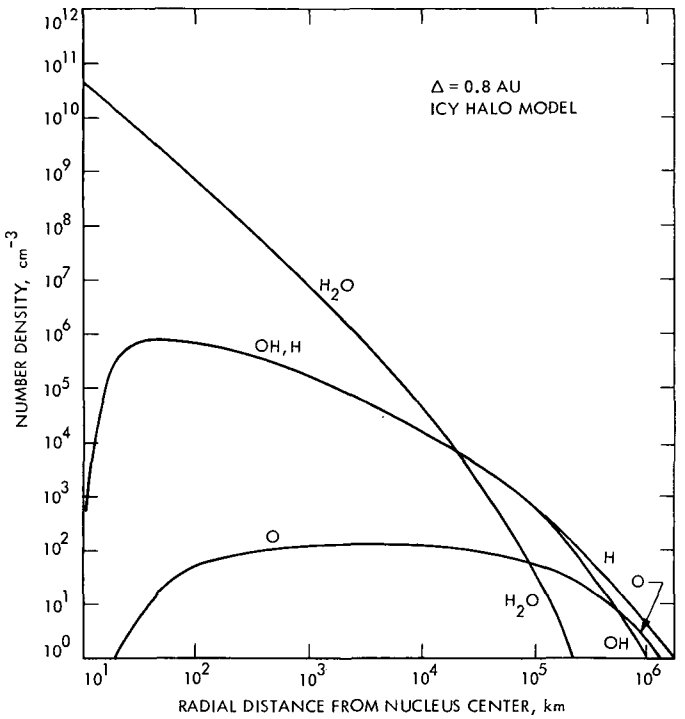

Fig. 15. Distribution of H_2O and its daughter products as a function of distance from the nucleus for a model with a halo of icy grains extending to 10^3 km, forming an extended source for H_2O (after D. M. Wexler)

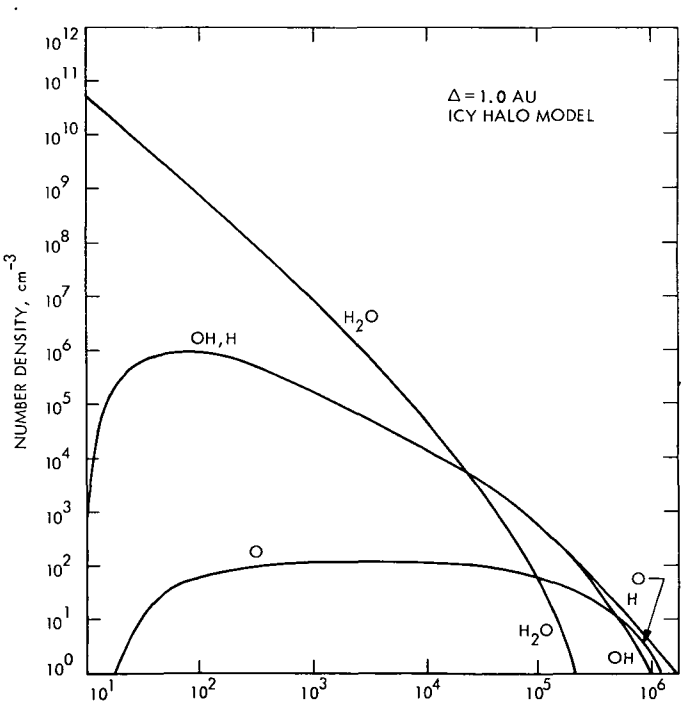

Fig. 16. Distribution of H_2O and its daughter products as a function of distance from the nucleus for an icy halo model at a heliocentric distance of 1 AU

The curves are easily scaled to other heliocentric distances as follows. The H_2O emission rate is expected to be proportional to the isolation, so that the densities will follow a simple inverse square law. The velocities are assumed to follow an inverse fourth root law. This follows if the temperature of the nucleus is determined by the usual gray body law

$$\epsilon \sigma T^4 = I(\Delta) \tag{2}$$

Where ϵ is the effective emissivity of the comet, σ is Stefan's constant, and I is the solar flux. Since I is proportional to Δ^{-2} and the velocity v is proportional to $T^{1/2}$ according to the kinetic theory, then

$$v \propto T^{1/2} \propto \Delta^{1/4} \tag{3}$$

The density profiles for C_3, C_2, CN, NH, NH_2, and CH, which appear in Fig. 17, are extremely tentative. They were obtained from estimates of the brightness of the principal emissions in various cometary spectra (including but not restricted to Encke) from Ref. 33. The absolute number densities were obtained for C_2 from the analysis of Section IV-C, and for the other species by estimating relative brightnesses, with due allowances for the different f-values (oscillator strengths). The spatial distributions were obtained very crudely by examining the intensity variation from the center to the edge of the head of the comet in the individual spectral lines. The results for CN and C_2 are very close to those estimated independently (and from different data) by Maines et al. (Ref. 7) over the range 3.81×10^4 to 8.87×10^4 km.

D. Model of the Icy Halo

Delsemme and Miller (Ref. 16) have presented an analysis of the production mechanism, dynamics, and evolution of icy grains in a model comet, based on laboratory studies of the behavior of the clathrate hydrate of methane under cometary conditions. This can be used to produce a model of the halo of icy grains, which, it is postulated, makes up the inner coma of Encke.

1. Properties of individual grains. The size distribution of grains of the clathrate hydrate of methane obtained under cometary conditions in the laboratory is shown in Fig. 18. The mean diameter is 0.6 mm, and the densities of individual grains fall in the range 0.33–0.54 g-cm^{-3}. The properties of other clathrate hydrates are similar to these, so the mean mass of an icy grain stripped from the nucleus of Encke may be taken to be approximately 5×10^{-5} g.

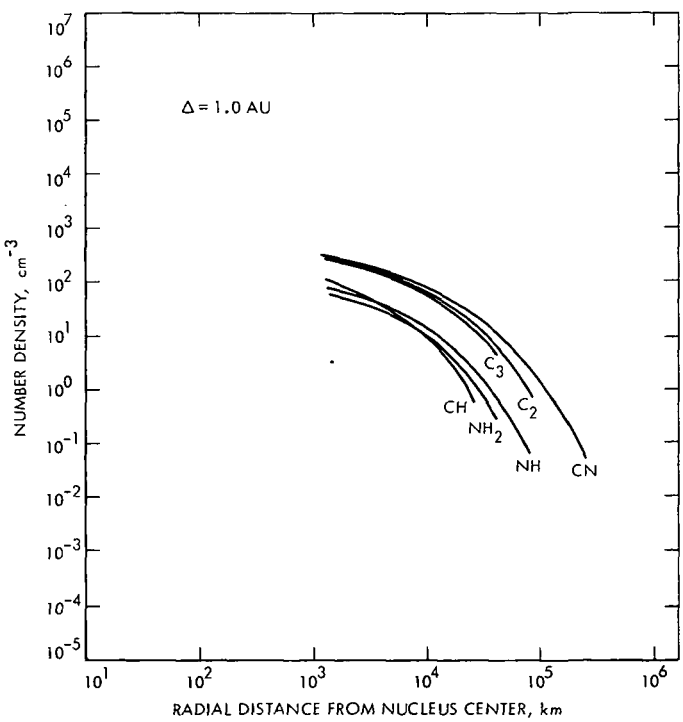

Fig. 17. Radial density distributions for six species at a heliocentric distance of 1 AU

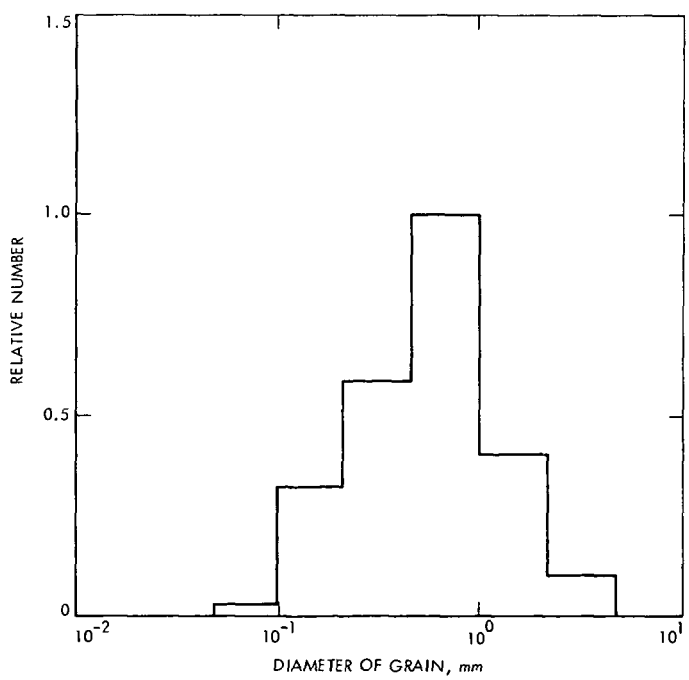

Fig. 18. Size distribution of icy grains of the clathrate hydrate of methane (Ref. 14)

2. Rate of production of grains. From their laboratory experiment, Delsemme and Miller (Ref. 16) estimated the ratio of the rate at which mass is lost as grains to that lost as gas to be 0.63. From Roemer's observations of comet Burnham (1960 II), they found a value of 0.43, which is consistent with the first value within the uncertainty of these estimates. The second value was obtained assuming that all of the continuum intensity in Burnham was due to reflection from grains, that the grains had the same albedo as the nucleus, and that the nuclear radius of Burnham is 2 km. Taking 0.5 as a working value for this ratio and assuming it applies to Encke also, it follows that one-third of the emission is in the form of icy grains and the remainder as gas. Adopting Sekanina's (Ref. 31) value of 10^{13} g per revolution for the rate of mass loss from Encke, the mean rate of grain production during the 100-day active phase is of the order of 10^{10} s^{-1}.

3. Grain velocities. Delsemme and Miller analyze at some length the dynamics of icy grains accelerated by the escaping gas. Adaption of their results to the present model of Encke results in the curve of Fig. 19 for the velocity of a grain as a function of time since leaving the nucleus. From this it can be seen that they reach a terminal velocity of about 15 m-s^{-1} at a distance of the order of 1 nuclear radius from the surface.

4. Grain lifetimes and extent of the halo. After reaching their terminal velocity, the grains continue to travel away from the nucleus until they evaporate completely. The time taken for the largest grain to vanish determines the extent of the halo.

The lifetime of a grain of albedo A_g, density ρ, and radius a_g is

$$\tau = \frac{\rho}{m}\frac{a_g}{z}\frac{1}{1-A_g} \qquad (4)$$

where m is the molecular mass and z mol-cm^{-2}-s^{-1} is the evaporation rate equal to $10^{17.2}$ at 1 AU for water ice (Ref. 16). Using Wenger's value of 0.9 for the mean albedo of a clathrate grain, we find $\tau \simeq 20$ h for a grain of radius 1 mm. Thus a halo diameter of approximately 10^3 km is predicted for Encke at 1 AU.

The variation in the halo diameter with heliocentric distance appears in Fig. 20. This is adapted from Delsemme and Miller's hydrodynamical calculations, which assumed the presence of some free methane in the nucleus. Since Encke is an old comet, any free methane it may have had is probably depleted. Delsemme and

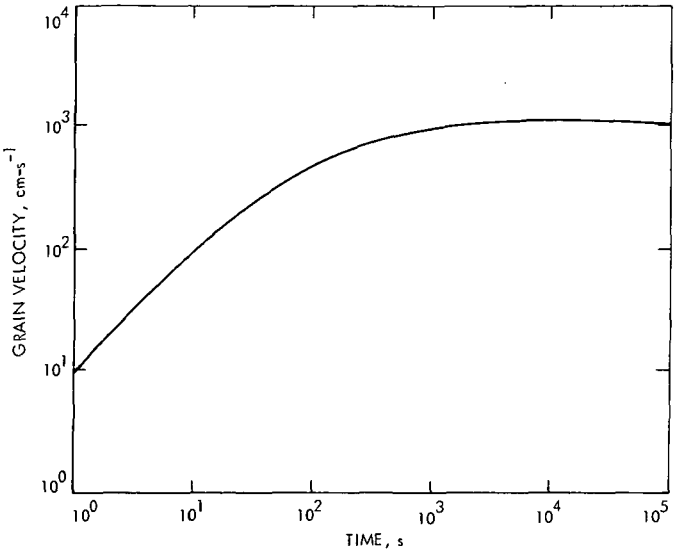

Fig. 19. Mean velocity of icy grains as a function of time elapsed since leaving the nucleus (after Ref. 16)

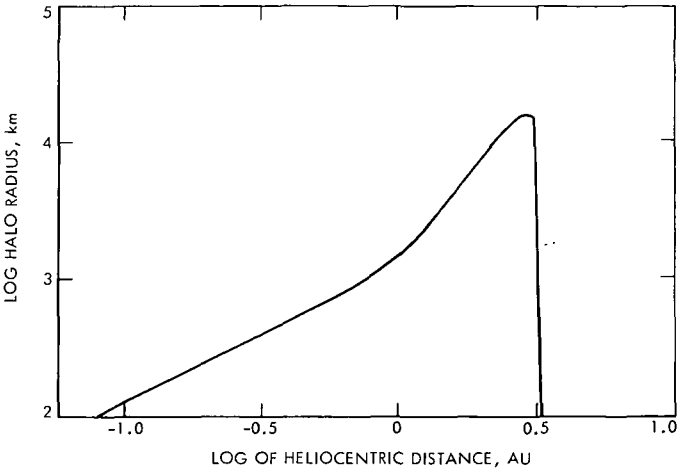

Fig. 20. Radius of icy halo as a function of heliocentric distance (after Ref. 16)

Miller's results have been modified to take account of this and to allow for a nuclear radius of 1.3 km rather than 2 km. The sharp disappearance of the halo near 3 AU corresponds to the point at which the grains are no longer able to escape against gravity.

E. Dust and Debris Model

This section treats the nonvolatile component of the material expelled by Encke. Dust (radius ≤ 100 μm) and debris (particles larger than 100 μm radius) are treated separately. The dust size distribution is estimated from

optical measurements following Finson and Probstein (Ref. 34) and the debris size distribution from estimates of the mass distribution in the Taurid meteor showers. The results overlap in the region of 100 μm radius and can be fitted together to give a single curve. The total integrated mass is then equated to Sekanina's (Ref. 31) estimate of the rate of mass loss from Encke to obtain absolute emission rates as a function of particle size.

1. Theory for debris. Whipple (Ref. 19) and Opik (Ref. 18) have presented evidence which strongly indicates that the Taurid meteor showers consist of particles expelled from Encke. Here it is assumed that the size distribution in the shower is the same as that in the present-day atmosphere of Encke during the active phase. Lovell (Ref. 35) gives the total mass in the β-Taurid shower as a function of optical magnitude. The magnitudes can be converted to mass values for individual meteorites using the rule given by Millman and McKinley (Ref. 36), which is

$$\text{mass} \propto \text{luminosity}$$

and

$$\text{zero magnitude} \equiv 1 \text{ g}$$

Next the density of the meteor is taken to be 3.4 g-cm^{-3} and a spherical shape assumed in order to obtain the radius. The density value is taken as typical for stone (Ref. 18). The use of a largish value for density is supported by the fact that the Taurid meteors are observed to be tough, i.e., not prone to fragmentation, in common with other debris of old comets (Ref. 21).

The results of this analysis appear in Table 8. Figure 21 shows a smooth curve drawn through the points, for purposes of interpolation.

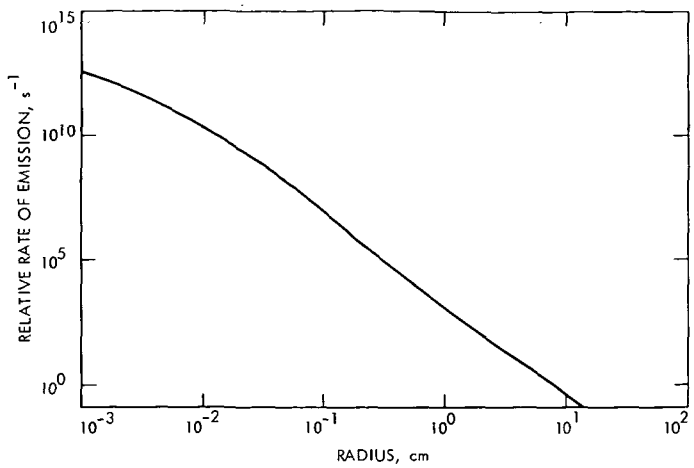

Fig. 21. Rate of emission of solid particles as a function of radius as inferred from meteor data

2. Upper limit on radius. Opik (Ref. 18) also calculates the maximum diameter of a particle expelled from Encke by a vapor jet working against gravity. Following his analysis,

$$\text{maximum } a = \frac{17.3}{\Delta^2 r} \text{ cm} \qquad (5)$$

where Δ is the heliocentric distance and r the radius of the nucleus. Inserting $r = 1.3$ km, we find the maximum radius of ejecta is of the order of 10 cm at 1.0 AU. This is consistent with the assumption that the mean mass of all meteors in the magnitude range < -10 is 2×10^4 g, which corresponds to a mean radius of 11 cm in this range and an upper cutoff of 13-cm radius. This value is also consistent with the independent estimate of 10^4 g as the order of magnitude of the mass of the largest fireballs in the Taurid stream photographed by the Smithsonian Astrophysical Observatory (Ref. 37).

Table 8. Statistics of the Taurid meteor showers

Magnitude range	Corresponding mass range, g	Mean mass of a meteor m, g	Mean radius of a meteor a, cm	Relative mass entering atmosphere	Relative number entering atmosphere
<-10	$>10^4$	2×10^4	11	1	1
-4 to -9	40–4000	400	3	0.2188	10
-3 to $+9$	2.5×10^{-4}–16	8	0.8	0.4725	1000
$+10$ to $+30$	10^{-12}–10^{-4}	10^{-8}	10^{-3}	0.7312	1.5×10^{12}

3. **Theory for dust.** The results of Finson and Probstein (Ref. 38) for comet Arend–Roland are adopted directly and scaled to fit Encke. Thus it is assumed that the principal difference between the two comets is one of total amount of dust emission rather than size distribution. The curve is modified slightly at the small particle end to correspond to a minimum particle radius of 0.3 μm (see next section). The results appear in Fig. 22.

4. **Lower limit on radius, a_{min}.** Assuming a particle density of 3.4 g-cm^{-2}, Finson and Probstein's results for Arend–Roland correspond to a minimum particle radius of approximately 0.7 μm. Sekanina and Miller (Ref. 39), using a similar analysis, found a value $a_{min} \simeq 0.3$ μm in comet Bennett (1970 II). The latter value has been adopted for Encke: $a_{min} = 3 \times 10^{-5}$ cm.

5. **Size distribution.** The overall size distribution is obtained by fitting the dust and debris curves (Figs. 21 and 22) to each other in the region of overlap. The scale giving the absolute number of particles per second in each size range is obtained by summing the mass–frequency product of each segment and equating it to the total rate of nonvolatile mass loss from Encke. To obtain the latter, Sekanina's (Ref. 40) value of 10^{13} g per orbit is assumed to consist of 10% nonvolatiles and to take place over 100 days, which is the period during which Encke is active. This gives a mean loss rate of 10^5 g-s^{-1} for rocky material. We assume that this mean rate is the one appropriate to the comet at ~0.7–1 AU (it will clearly be higher at perihelion and lower at distances close to the onset of activity, see Section III-E-9). It is then consistent with the OGO-5 observations of the rate of expulsion of hydrogen atoms from Encke (Ref. 29), provided that the majority of the remaining 90% of the mass lost is H_2O. Normalizing the curve to this value, we obtain the results which are tabulated in Table 9 and presented graphically in Fig. 23.

6. **Velocity distribution.** The dynamics of solid particles accelerated by the jet of escaping vapor from the nucleus has been treated by Probstein (Ref. 41) and by Delsemme and Miller (Ref. 16). Probstein shows that small grains (i.e., millimeter size or less) attain their terminal velocities in times of the order of 100 s, i.e., very soon after leaving the nucleus and in distances of less than 1 nuclear radius. Delsemme and Miller confirm this result and show that even very large grains reach their terminal velocity within 10^3 or 10^4 s and in distances of the order of 10 nuclear radii. The actual value of the terminal velocity is a function of the gravitational field of the nucleus (i.e., its mass) and of the evaporation rate of the volatiles. Figure 24 shows the terminal velocity as a function of particle radius for Encke, assuming a radius of 1.3 km, a mean density of 1 g-cm^{-3}, and the evaporation rate appropriate to solid H_2O at 1 AU from the Sun.

7. **Radial distribution of particles.** The discussion of Section III-E-6 indicates that all particles move through the coma at a constant velocity except very near the nucleus. Thus the number density for a given radius will follow an inverse square-law distribution with distance

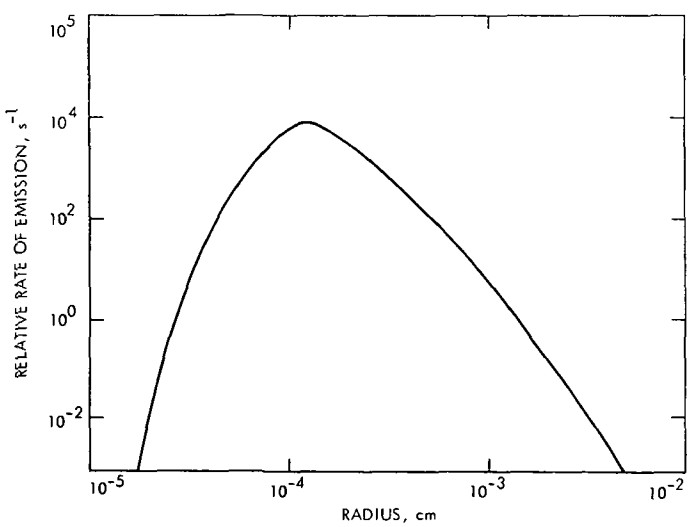

Fig. 22. Rate of emission of solid particles as a function of radius adapted from Finson and Probstein (Ref. 38) and Sekanina and Miller (Ref. 39)

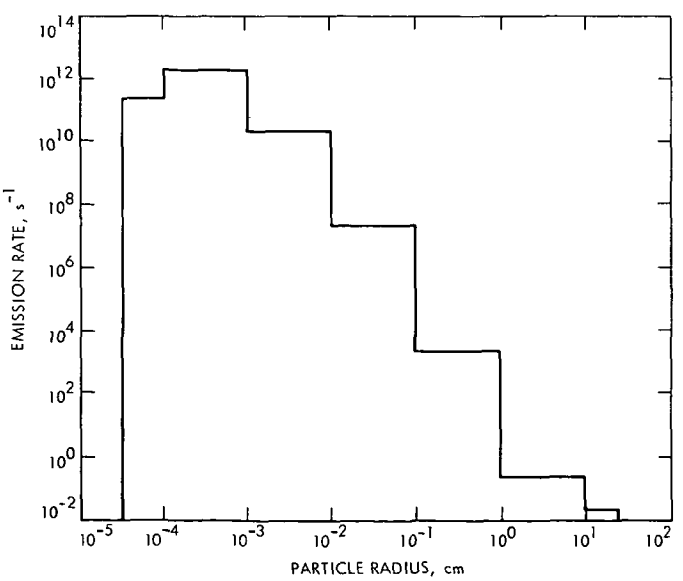

Fig. 23. Emission rate of particles as a function of size

Table 9. Rate of emission of particles as a function of size

Size range, cm	Mean mass, g	Rate of particle emission, s^{-1}	Rate of mass emission, $g\text{-}s^{-1}$
$<3 \times 10^{-5}$	0	0	0
3×10^{-5}–10^{-4}	3×10^{-12}	2.5×10^{11}	7.5×10^{-1}
10^{-4}–10^{-3}	2×10^{-9}	2.5×10^{12}	5×10^{3}
10^{-3}–10^{-2}	2×10^{-6}	2.5×10^{10}	5×10^{4}
10^{-2}–10^{-1}	2×10^{-3}	2.5×10^{7}	5×10^{4}
10^{-1}–1	2	2.5×10^{3}	5×10^{3}
1–10	2×10^{3}	2.5×10^{-1}	5×10^{2}
10–25	3×10^{4}	2.5×10^{-2}	7.5×10^{1}
			Total $\approx 10^{5}$ $g\text{-}s^{-1}$

from the nucleus in the coma. This situation will be perturbed somewhat by the force on the particles due to solar radiation, which tends to sweep the dust back into a type II tail. The fact that such a tail has never been observed in Encke sets an upper limit on the rate of dust emission, as discussed in the following section.

8. Upper limits on dust content. If it is assumed that the mean rate of mass loss of 10^5 $g\text{-}s^{-1}$ due to rocky material is all given off as 1-μm radius dust particles, the emission rate is

$$n = \frac{\text{rate of mass loss}}{\text{mass of a particle}} = \frac{10^5}{\frac{4}{3}\pi (10^{-4})^3\, 3.4} \simeq 7 \times 10^{15} \text{ particles per second} \quad (6)$$

which corresponds to a total rate approximately 2×10^3 times higher than the nominal model predicts.

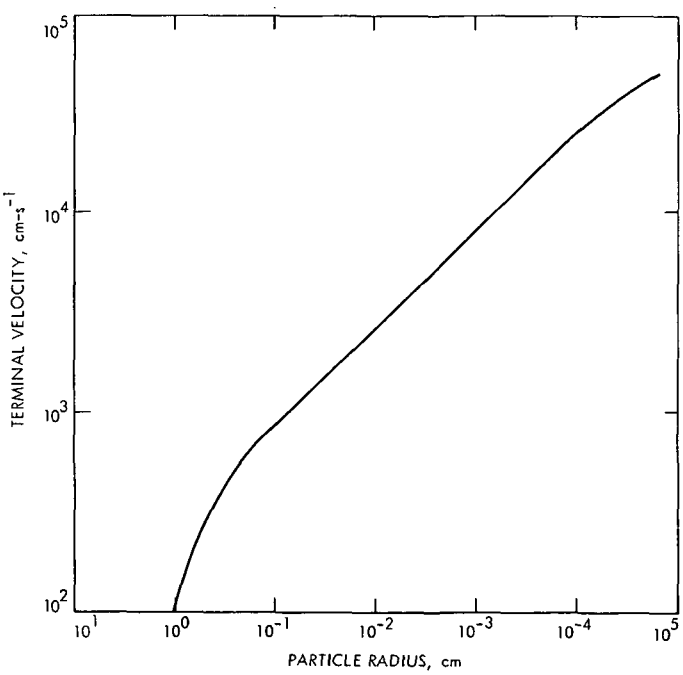

Fig. 24. Terminal velocity of solid particles at 1 AU as a function of radius (after Ref. 16)

A second estimate of the upper limit can be established by considering the dust content required to produce the observed continuum intensity. This is given by Liller (Ref. 33) as $<1/5$ of the intensity of the 5165-Å C_2 band, which is consistent with plate 16 of the *Atlas of Representative Cometary Spectra* (Ref. 33). It can be seen from this plate, however, that the continuum is not entirely undetected and for the purpose of the present calculations we will take the ratio [C_2 band intensity]/[continuum intensity] = 10. Multiplying by the relative effective spectral widths, we get the ratio [C_2 band energy in V passband]/[continuum energy in V passband] $\approx 10 \times 0.016/0.032 = 5$. Thus about 20% of the observed brightness of Encke in the V passband could be due to reflection from dust. Note, however, that the coma is expected to contain an extensive halo of icy grains. These will also scatter sunlight, and with a higher albedo than dust particles. For purposes of establishing an upper limit, however, it will be assumed that all of the observed continuum is due to dust.

In the absence of factual information on the scattering properties of the dust particles, isotropic and conservative scattering will be assumed as the simplest model. Measurements by Richter (Ref. 42) show that dielectric particles of ~1-μm radius do scatter almost isotropically, while the results of Peterson and Weinman (Ref. 43), based on measurements of Spitzer and Kleinman (Ref. 44), show a single-scattering albedo of 1 (conservative scattering) for polydispersions of quartz dust at near-visible infrared wavelengths.

Then we can write

$$\text{Brightness of Encke} = \text{brightness of Sun} \times \frac{\text{total cross-section of dust}}{4\pi\,(\text{comet–Sun distance})^2} \tag{7}$$

Assuming that the coma is optically thin, then

$$B_{\mathfrak{R}} = B_{\odot} \times \frac{\Sigma\, n\, \pi\, a^2 \times \dfrac{D}{2v} \times \ell}{4\,\pi\,\Delta^2} \tag{8}$$

where

$B_{\mathfrak{R}}$ = brightness of comet

$B_{\odot}$ = brightness of Sun

n = number of particles per second in a given size range

a = mean particle radius in a given size range

D = diameter of coma

v = velocity of dust particles during traversal of coma

ℓ = length of comet along axis of tail in units of the diameter of the head

Δ = comet–Sun distance

This formula assumes that all of the dust is swept into the tail before it reaches a distance r from the nucleus; r is taken equal to the coma radius, 10^5 km. The parameter ℓ expresses how long the dust remains a part of the observed comet before dissipating away. Observations of Encke show the continuum decreasing in intensity very rapidly with distance from the nucleus, and no dust tail at all. There does not appear to be any contribution to the recorded continuum from outside the head of the comet, so ℓ will be set equal to 1. Inserting this value and $D = 10^5$ km, $v = 400$ m-s^{-1}, $R = 1$ AU, and $\Sigma na^2 \simeq 10^6$ cm^2-s^{-1} (from the nominal dust model), we obtain

$$B_{\mathfrak{R}} \simeq B_{\odot} \times 10^{-16} \tag{9}$$

Note also that

$$\frac{\Sigma\, n\, \pi\, a^2 \times \dfrac{D}{2v} \times \ell}{\pi \left(\dfrac{D}{2}\right)^2} \simeq 10^{-9} \ll 1 \tag{10}$$

confirming the use of an optically thin model for the dust. The result (9) is compared to the observations as follows. The magnitude of the Sun in the V passband is -26.8. The magnitude of Encke in the same passband at 1 AU from the Sun is 11.1 (Section IV-B). So the relative brightnesses are

$$\frac{B_{\odot}}{B_{\mathfrak{R}}} = \log_{10}^{-1}\left[-0.4\,(-26.8 - 11.1)\right] \simeq 2 \times 10^{15} \tag{11}$$

If 20% of the brightness of Encke is due to dust, then the factor $B_{\odot}/B_{\mathfrak{R}}$ (dust) is 10^{16}, or exactly the value predicted by the nominal dust model.

A similar analysis to the above has been performed by Maines et al. (Ref. 7), except that they considered three hypothetical cases for monodispersions of radius 0.36, 0.19, and 0.055 μm. Although it is unlikely that most of the mass loss from Encke could be in the form of particles this small, because of the meteoritic evidence and the analyses of Finson and Probstein (Refs. 34 and 38) and of Sekanina and Miller (Ref. 39), it is interesting to compare this result to the above, particularly since they are based on independent observational data. All of Maines' results can be scaled to a single value for $N(1\ \mu\text{m})$, which is the total emission rate (s^{-1}) of particles required to explain their observed continuum if all particles are of radius 1 μm. The result is $N(1\ \mu\text{m}) \simeq 5.6 \times 10^{13}$ s^{-1}. Repeating the calculations of the preceding paragraph for a 1-μm monodispersion instead of the nominal dust model, we find $N(1\ \mu\text{m}) \simeq 10^{14}$ s^{-1}. This demonstrates consistency between the independent calculations.

Since the continuum scattering calculations verify the nominal dust model, the principal factor determining the upper limit on the amount of dust in the model is the

uncertainty in the total rate of mass emission and its distribution between gas, ices, and dust. The former is uncertain by roughly one order of magnitude (Ref. 31) and the latter by about the same amount. The radius at which the size distribution in Fig. 23 peaks is uncertain by at least a factor of 2, which is equivalent to another order of magnitude in n. Therefore, a reasonable limit on the dust abundance is a factor 10^3 times the entries in the nominal model. This is approximately equal to the upper limit established above for the case of all of the nonvolatile emission being fine dust.

A lower limit on the dust content of Encke is no dust at all. Although the Taurid meteor shower almost certainly has its origin in material expelled from Encke, there is no way to say in which epoch this expulsion occurred. There is no observational evidence for the presence of dust in Encke at the present time, except for the presence of a faint reflected solar continuum. As noted above, some or all of the continuum is probably due to reflection from icy grains in the inner coma and no definite conclusion concerning the presence of dust is possible. It seems reasonable, however, given that Encke has at some time expelled large amounts of nonvolatiles and that the comet is still active, to assume that a nonnegligible emission of dust still takes place. A reasonable working lower limit for the abundance of dust is a factor 10^{-3} times the values in the nominal model.

9. Heliocentric dependence of dust model. The nominal dust and debris model applies to heliocentric distances in the region of 1 AU. Both the rate of emission of particles and the maximum size of particles will increase near perihelion and tend to vanish near aphelion. The rate of emission probably depends on the rate of evaporation of ices and, therefore, should follow an inverse square law with distance from the Sun. Thus the rates shown in Table 9 and Fig. 23 may be expected to increase by about an order of magnitude at perihelion, and the maximum particle size to around 1 m in diameter if particles of such a size are present in Encke. The evidence from the Taurid meteor streams implies that if they do occur, they are extremely rare. Since evaporation is a threshold effect, the dust emission will fall to zero beyond about 2 AU if the expulsion is driven by evaporation of H_2O. Since the visual activity of Encke shows a considerable decrease after perihelion compared with before, the amount of gas available to expel dust will show the same asymmetry.

In general the expected heliocentric dependence of the dust model falls within the boundaries of uncertainty on the nominal model, which would make any attempt to generate a Δ-dependence model unprofitable.

F. Impact Model

The rate of impact of dust particles on a body near the comet is an important quantity for spacecraft design. This quantity is evaluated here for a cross-sectional area of 10 m^2 (appropriate to a Mariner-sized spacecraft) and for the slow flyby trajectory of Fig. 25 (Ref. 45). The particle velocities of Fig. 24 are assumed; the trajectory does not approach closely enough to the nucleus for impacts by dust particles at less than their terminal velocity or by icy grains to occur. The calculations are repeated for two models of the particle structure of Encke (Fig. 26); the first is completely spherically symmetric while the second assumes spherical symmetry out to the boundary of the coma ($r = 10^5$ km), whereafter all of the dust is swept into a homogeneous dust tail. In each case the enhancement of the impact rate due to the component of the velocity of the spacecraft along the radial direction is included. This is positive during approach and negative after encounter, and is responsible for the asymmetry of the impact profiles. The rates of impact are calculated from the nominal dust model (Section III-E) and are, therefore, subject to the range of uncertainties discussed in Section III-E-8. The results are tabulated for individual ranges of particle radius in Tables 10 and 11, and the total impact rate is presented graphically in Figs. 27 and 28.

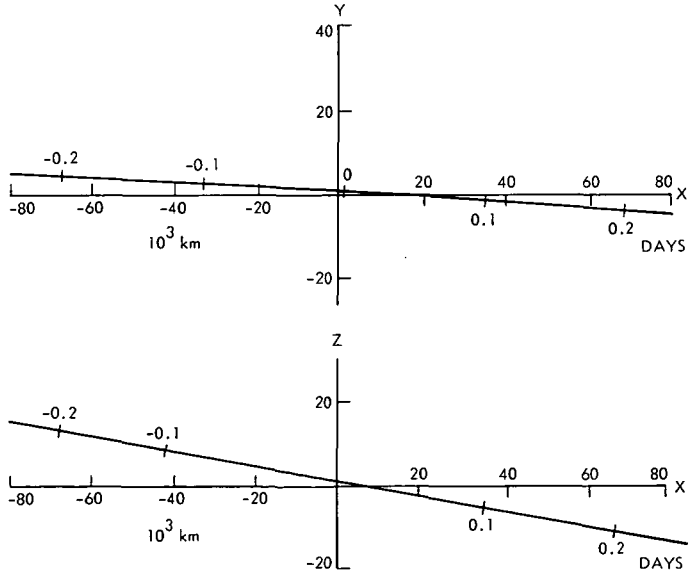

Fig. 25. Trajectory for Encke slow flyby used in computing impact models (Ref. 45)

(a) SYMMETRIC MODEL

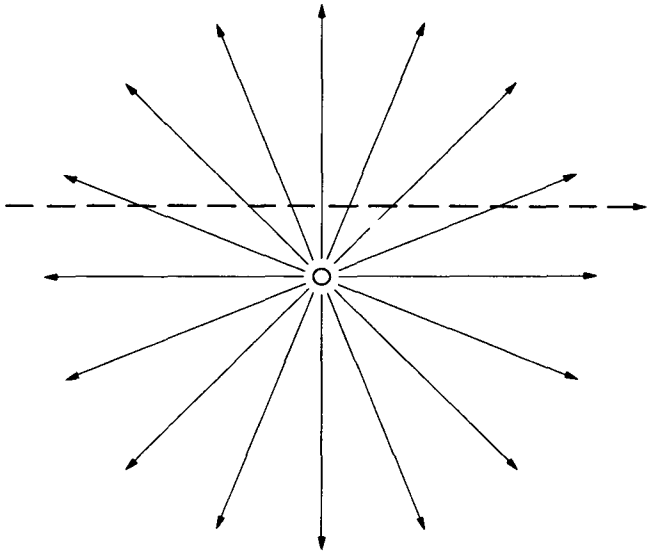

(b) HOMOGENEOUS TAIL MODEL

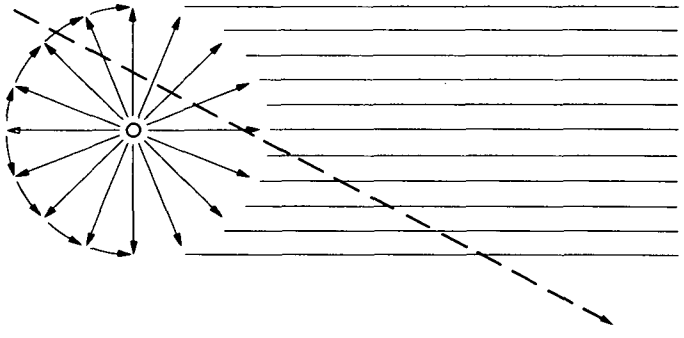

Fig. 26. Models of the structure of the dust component of Encke used in calculating the impact models. The spacecraft trajectory is shown schematically (see also Fig. 26); the velocity is 4 km-s^{-1} and the distance of closest approach is 10^3 km in both cases

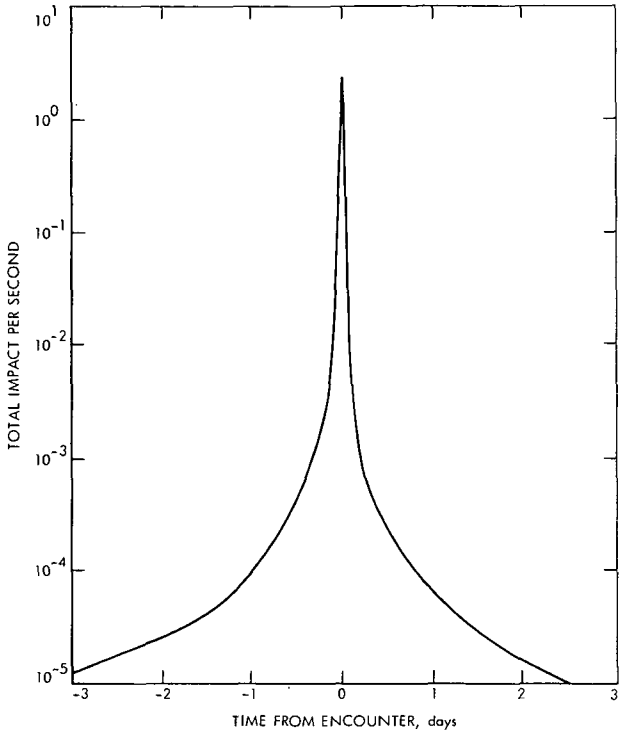

Fig. 27. Impact model for a spacecraft of 10-m^2 cross section traveling at 4 m-s^{-1} through the symmetric dust model (encounter distance = 10^3 km)

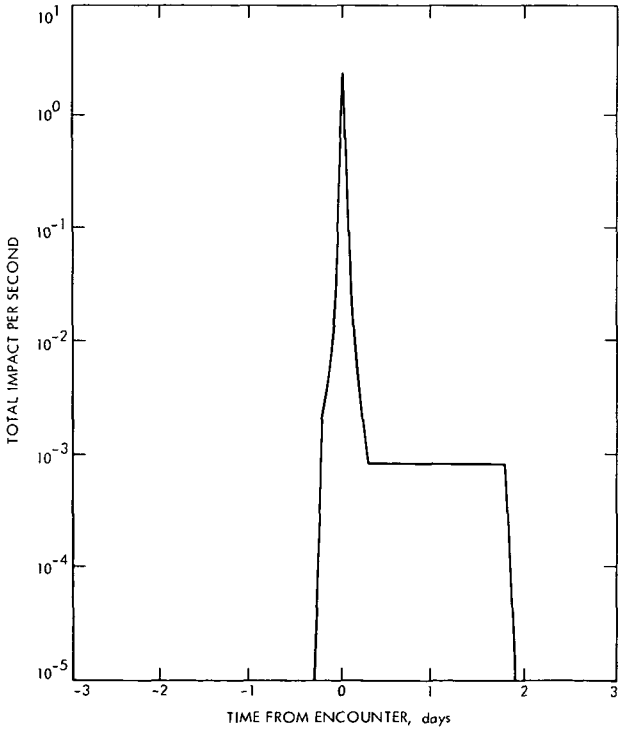

Fig. 28. Impact model for trajectory of Fig. 25 and symmetric tail model of Encke

Table 10. Impact model for symmetric model of comet

NUMBER OF COLLISIONS PER SEC WITH AN AREA OF 10 SQ METERS AS A FUNCTION OF TIME FROM ENCOUNTER

		PARTICLE RADIUS RANGE IN CM.						
TIME (DAYS)	DISTANCE (KM)	E-5 TO E-3	E-3 TO E-2	E-2 TO E-1	E-1 TO 1	1 TO 10	10 TO 25	TOTAL
-2.50	864000.57	.163-04	.350-06	.847-09	.263-12	.107-15	.107-15	.166-04
-2.40	829440.59	.176-04	.379-06	.919-09	.285-12	.116-15	.116-15	.180-04
-2.30	794880.62	.192-04	.413-06	.100-08	.310-12	.126-15	.126-15	.196-04
-2.20	760320.65	.210-04	.452-06	.109-08	.339-12	.138-15	.138-15	.215-04
-2.10	725760.68	.231-04	.496-06	.120-08	.372-12	.151-15	.151-15	.235-04
-2.00	691200.71	.254-04	.546-06	.132-08	.410-12	.167-15	.167-15	.260-04
-1.90	656640.75	.282-04	.605-06	.147-08	.455-12	.185-15	.185-15	.288-04
-1.80	622080.80	.314-04	.675-06	.163-08	.507-12	.206-15	.206-15	.321-04
-1.70	587520.84	.352-04	.756-06	.183-08	.568-12	.231-15	.231-15	.359-04
-1.60	552960.91	.397-04	.854-06	.207-08	.641-12	.261-15	.260-15	.406-04
-1.50	518400.96	.452-04	.971-06	.235-08	.730-12	.297-15	.296-15	.462-04
-1.40	483841.03	.519-04	.112-05	.270-08	.838-12	.341-15	.340-15	.530-04
-1.30	449281.11	.602-04	.129-05	.313-08	.971-12	.395-15	.394-15	.614-04
-1.20	414721.20	.706-04	.152-05	.367-08	.114-11	.464-15	.463-15	.721-04
-1.10	380161.31	.840-04	.181-05	.437-08	.136-11	.552-15	.551-15	.858-04
-1.00	345601.44	.102-03	.219-05	.529-08	.164-11	.668-15	.666-15	.104-03
-.90	311041.60	.126-03	.270-05	.653-08	.203-11	.825-15	.823-15	.128-03
-.80	276481.81	.159-03	.341-05	.827-08	.257-11	.104-14	.104-14	.162-03
-.70	241922.07	.207-03	.446-05	.108-07	.335-11	.136-14	.136-14	.212-03
-.60	207362.42	.282-03	.607-05	.147-07	.456-11	.186-14	.185-14	.288-03
-.50	172802.90	.407-03	.874-05	.212-07	.657-11	.267-14	.267-14	.415-03
-.40	138243.62	.635-03	.137-04	.331-07	.103-10	.417-14	.416-14	.649-03
-.30	103684.83	.113-02	.243-04	.588-07	.182-10	.742-14	.740-14	.115-02
-.20	69127.24	.254-02	.546-04	.132-06	.410-10	.167-13	.167-13	.260-02
-.10	34574.47	.102-01	.218-03	.529-06	.164-09	.667-13	.666-13	.104-01
-.00	1000.00	.260+01	.307-01	.473-04	.107-07	.376-11	.358-11	.263+01
.10	34574.46	.656-02	.185-03	.495-06	.161-09	.664-13	.665-13	.674-02
.20	69127.23	.164-02	.463-04	.124-06	.402-10	.166-13	.166-13	.169-02
.30	103684.81	.730-03	.206-04	.551-07	.179-10	.738-14	.740-14	.750-03
.40	138243.60	.410-03	.116-04	.310-07	.101-10	.415-14	.416-14	.422-03
.50	172802.88	.263-03	.741-05	.198-07	.643-11	.266-14	.266-14	.270-03
.60	207362.40	.182-03	.515-05	.138-07	.447-11	.185-14	.185-14	.188-03
.70	241922.06	.134-03	.378-05	.101-07	.328-11	.136-14	.136-14	.138-03
.80	276481.79	.103-03	.289-05	.775-08	.251-11	.104-14	.104-14	.106-03
.90	311041.59	.811-04	.229-05	.612-08	.199-11	.820-15	.822-15	.834-04
1.00	345601.43	.657-04	.185-05	.496-08	.161-11	.665-15	.666-15	.675-04
1.10	380161.29	.543-04	.153-05	.410-08	.133-11	.549-15	.550-15	.558-04
1.20	414721.19	.456-04	.129-05	.344-08	.112-11	.462-15	.463-15	.469-04
1.30	449281.10	.389-04	.110-05	.293-08	.952-12	.393-15	.394-15	.400-04
1.40	483841.02	.335-04	.945-06	.253-08	.821-12	.339-15	.340-15	.345-04
1.50	518400.96	.292-04	.823-06	.220-08	.715-12	.295-15	.296-15	.300-04
1.60	552960.87	.257-04	.724-06	.194-08	.628-12	.260-15	.260-15	.264-04
1.70	587520.84	.227-04	.641-06	.172-08	.557-12	.230-15	.230-15	.234-04
1.80	622080.80	.203-04	.572-06	.153-08	.496-12	.205-15	.206-15	.208-04
1.90	656640.73	.182-04	.513-06	.137-08	.446-12	.184-15	.185-15	.187-04
2.00	691200.71	.164-04	.463-06	.124-08	.402-12	.166-15	.167-15	.169-04
2.10	725760.66	.149-04	.420-06	.112-08	.365-12	.151-15	.151-15	.153-04
2.20	760320.64	.136-04	.383-06	.102-08	.332-12	.137-15	.138-15	.140-04
2.30	794880.62	.124-04	.350-06	.937-09	.304-12	.126-15	.126-15	.128-04
2.40	829440.58	.114-04	.322-06	.861-09	.279-12	.115-15	.116-15	.117-04
2.50	864000.57	.105-04	.296-06	.793-09	.257-12	.106-15	.107-15	.108-04

Table 11. Impact model for asymmetric model of comet

NUMBER OF COLLISIONS PER SEC WITH AN AREA OF 10 SQ METERS AS A FUNCTION OF TIME FROM ENCOUNTER

		PARTICLE RADIUS RANGE IN CM.						
TIME (DAYS)	DISTANCE (KM)	E-5 TO E-3	E-3 TO E-2	E-2 TO E-1	E-1 TO 1	1 TO 10	10 TO 25	TOTAL
-2.50	840633.73	.000	.000	.000	.000	.000	.000	.000
-2.40	807016.03	.000	.000	.000	.000	.000	.000	.000
-2.30	773398.30	.000	.000	.000	.000	.000	.000	.000
-2.20	739780.61	.000	.000	.000	.000	.000	.000	.000
-2.10	706162.91	.000	.000	.000	.000	.000	.000	.000
-2.00	672545.21	.000	.000	.000	.000	.000	.000	.000
-1.90	638927.52	.000	.000	.000	.000	.000	.000	.000
-1.80	605309.82	.000	.000	.000	.000	.000	.000	.000
-1.70	571692.13	.000	.000	.000	.000	.000	.000	.000
-1.60	538074.45	.000	.000	.000	.000	.000	.000	.000
-1.50	504456.77	.000	.000	.000	.000	.000	.000	.000
-1.40	470839.11	.000	.000	.000	.000	.000	.000	.000
-1.30	437221.46	.000	.000	.000	.000	.000	.000	.000
-1.20	403603.82	.000	.000	.000	.000	.000	.000	.000
-1.10	369986.19	.000	.000	.000	.000	.000	.000	.000
-1.00	336368.59	.000	.000	.000	.000	.000	.000	.000
-.90	302751.01	.000	.000	.000	.000	.000	.000	.000
-.80	269133.47	.000	.000	.000	.000	.000	.000	.000
-.70	235516.00	.000	.000	.000	.000	.000	.000	.000
-.60	201898.61	.000	.000	.000	.000	.000	.000	.000
-.50	168281.35	.000	.000	.000	.000	.000	.000	.000
-.40	134664.32	.000	.000	.000	.000	.000	.000	.000
-.30	101047.78	.000	.000	.000	.000	.000	.000	.000
-.20	67432.43	.267-02	.574-04	.139-06	.431-10	.175-13	.175-13	.273-02
-.10	33821.80	.106-01	.228-03	.552-06	.171-09	.697-13	.696-13	.108-01
-.00	1000.00	.260+01	.307-01	.473-04	.107-07	.376-11	.358-11	.263+01
.10	33442.34	.701-02	.198-03	.529-06	.172-09	.709-13	.711-13	.721-02
.20	67052.85	.174-02	.492-04	.132-06	.427-10	.177-13	.177-13	.179-02
.30	100668.18	.859-03	.796-05	.796-08	.796-12	.796-16	.796-17	.867-03
.40	134284.71	.859-03	.796-05	.796-08	.796-12	.796-16	.796-17	.867-03
.50	167901.72	.859-03	.796-05	.796-08	.796-12	.796-16	.796-17	.867-03
.60	201518.99	.859-03	.796-05	.796-08	.796-12	.796-16	.796-17	.867-03
.70	235136.38	.859-03	.796-05	.796-08	.796-12	.796-16	.796-17	.867-03
.80	268753.85	.859-03	.796-05	.796-08	.796-12	.796-16	.796-17	.867-03
.90	302371.38	.859-03	.796-05	.796-08	.796-12	.796-16	.796-17	.867-03
1.00	335988.96	.859-03	.796-05	.796-08	.796-12	.796-16	.796-17	.867-03
1.10	369606.55	.859-03	.796-05	.796-08	.796-12	.796-16	.796-17	.867-03
1.20	403224.19	.859-03	.796-05	.796-08	.796-12	.796-16	.796-17	.867-03
1.30	436841.84	.859-03	.796-05	.796-08	.796-12	.796-16	.796-17	.867-03
1.40	470459.48	.859-03	.796-05	.796-08	.796-12	.796-16	.796-17	.867-03
1.50	504077.16	.859-03	.796-05	.796-08	.796-12	.796-16	.796-17	.867-03
1.60	537694.82	.859-03	.796-05	.796-08	.796-12	.796-16	.796-17	.867-03
1.70	571312.52	.859-03	.796-05	.796-08	.796-12	.796-16	.796-17	.867-03
1.80	604930.20	.859-03	.796-05	.796-08	.796-12	.796-16	.796-17	.867-03
1.90	638547.88	.000	.000	.000	.000	.000	.000	.000
2.00	672165.60	.000	.000	.000	.000	.000	.000	.000
2.10	705783.27	.000	.000	.000	.000	.000	.000	.000
2.20	739400.98	.000	.000	.000	.000	.000	.000	.000
2.30	773018.70	.000	.000	.000	.000	.000	.000	.000
2.40	806636.40	.000	.000	.000	.000	.000	.000	.000
2.50	840254.13	.000	.000	.000	.000	.000	.000	.000

IV. Photometric Model

A. General

The spectrum of Encke is characterized by a very low level of continuum reflection due to the low rate of emission of dust and ice particles. The strongest band emitting visible light from Encke is the 0–0 Swan band in C_2 centered on 5165 Å. In the following analysis the rate of photon emission from Encke in this band is calculated, and the surface brightness of the coma computed. These relate to the brightnesses in the V passband of the UBV system, which takes in the 5165-Å band but no other bands of importance. The continuum contribution is neglected.

B. Total Visible Magnitude of Encke

The brightness of a comet on the heliocentric and geocentric distances Δ and δ according to the expression

$$B_{\mathfrak{P}} = \frac{B^0_{\mathfrak{P}}}{\delta^2 \Delta^q} \tag{12}$$

where the index q is different for each comet and must be determined empirically. Observational data fully justifies the use of such a law (Ref. 46). In terms of magnitudes

$$H = H_0 + 5 \log \delta + 2.5\, q \log \Delta \tag{13}$$

Fitting to all of the available observations of Encke gives

$$H = 11.1 + 5 \log \delta + 15 \log \Delta \tag{14}$$

where the value $H_0 = 11.1$ corresponds to the absolute magnitude scaled to the 1980 apparition, assuming that the observed rate of decline of 0.1 magnitude per orbit will be maintained (Section IV-F).

C. Surface Brightness

The surface brightness of Encke is calculated from the absolute visual magnitude and the known f-value and relative transition probability for the 0–0 band of C_2, following the theory of Wurm (Ref. 47). First, the radiation temperature which determines the population of the upper levels is calculated (Eq. 6, Ref. 47), assuming radiative equilibrium with the Sun, to be 1650 K. The relative population of the upper level is then $n_r = 10^{-7.75}$.

The total output for a source at 1 AU is

$$E_0 = 10^{15.00} \times 10^{-0.4 H_0}\ \text{J-s}^{-1} \tag{15}$$

where H_0 is the absolute visual magnitude = 11.1 for Encke extrapolated to 1980, giving $E_0 = 10^{28.96}$ quanta per second.

E_0 is related to n_r via the Einstein coefficient $A(C_2)$ for the transition probability; $A(C_2)$ is given by the well-known formula

$$A(C_2) = 3\gamma f = 0.66\, \lambda^{-2} f\ \text{s}^{-1} \tag{16}$$

where γ is the classical damping coefficient. $f = 0.02$ for the Swan bands so $A(C_2) = 10^{6.75}\ \text{s}^{-1}$.

Now the total number of C_2 molecules in Encke in the ground state $N(C_2)$ can be calculated since

$$N(C_2) = \frac{E_0}{n_r A} = 10^{29.96}\ \text{molecules} \tag{17}$$

Assuming a density distribution of the form

$$d(C_2) = \frac{k}{r^2} \rho^{-\rho/\rho_0} \tag{18}$$

where r is distance from the center of the nucleus; the constant k is determined by integrating Eq. (18) through a sphere of radius $\rho_0 = 10^{10}$ cm and equating to Eq. (17). The result is $k = 10^{18.9}$. To form the emission law, k is multiplied by $k' = E^0/N(C_2)$ or the number of photons per second per molecule ($= 10^{0.1}$) and the density function projected onto the plane of the sky (Fig. 29); in terms of the projected distance $r' = r \sin \phi$, the density distribution of emitting molecules is

$$D(r') = \frac{k\, k'}{(r')^2 \csc^2 \phi} \rho^{-r' \csc \phi / r} \tag{19}$$

Assuming that the volume intensity of emission is proportional to the molecular density, the total intensity per unit area observed along the line of sight (or "surface brightness") is

$$I(r') = \frac{k\, k'}{r'} \int_\theta^\pi \rho^{-r' \csc \phi / r_0}\, d\phi \tag{20}$$

The surface brightness is calculated as a function of distance from the nucleus ρ and viewing angle θ by integration of Eq. (20) and is presented in Tables 12, 13, and 14.

D. Brightness at Other Wavelengths

The surface brightnesses in Tables 12, 13, and 14 will apply only to the V passband, which contains the 5165-Å C_2 band. Approximate multiplicative factors, which convert the tabulated brightnesses into the corresponding values for other passbands, are given in Table 15. It is assumed that any passband of interest either includes or excludes completely each of the emission lines, and the small continuum contribution is neglected. For passbands which include more than one emission band, the factors should be added together, e.g., the surface brightness of Encke in a 3050–3400-Å passband is 0.05 + 0.2 = 0.25 times the tabulated entry.

These relative brightnesses are taken from Ref. 7 for C_2 and CN and estimated from the spectra of Encke taken from Ref. 48 for other species. In the cases of OH^+ and CH^+, which have not been observed in Encke, estimates from the spectra of other, brighter, comets have been employed.

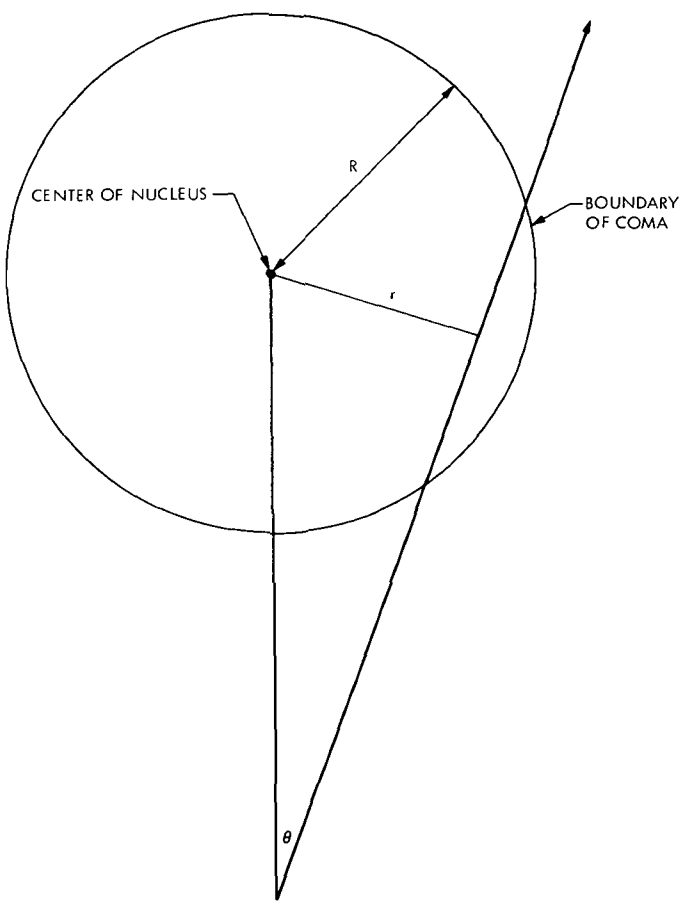

Fig. 29. Geometry assumed in calculation of the photometric model, defining the quantities *r*, *R*, and θ

E. Photometric Properties of the Halo in the Continuum

The model of Section III-D indicates an abundance of icy grains large enough to contribute an appreciable brightness to the continuum of Encke by the reflection of sunlight. Although the intensity in the continuum of Encke as observed from Earth is very low relative to many other comets, indicating a relatively low abundance of icy grains and dust, it is not completely absent. It should, therefore, be readily measurable by photometric instruments on comet mission spacecraft. It is not known at the present time what fraction of the observed continuum of Encke is due to dust and what fraction to icy grains, but the photometric profile of the continuum can be computed separately for each extreme. In fact the way in which the continuum intensity varies with distance from the nucleus is quite different in each case because the cross section of the scatterer is a function of radial distance in the case of grains but not for dust. The difference is such that even good ground-based photometric observations are diagnostic, as Delsemme and Miller (Ref. 16) have shown for O'Dell's (Ref. 49) observations of Comet Burnham (1960 II). Figure 30 shows the surface brightness of Encke in the continuum of the V passband as calculated from Delsemme and Miller's results, assuming in one case that the reflection is entirely from icy grains and in the other that it is entirely from dust.

The curve for the icy grains is calculated assuming that the cross-sectional area of a grain varies with distance r from the nucleus as

$$\sigma = \sigma_0 \left(1 - \frac{r}{R_H}\right)^2 \tag{21}$$

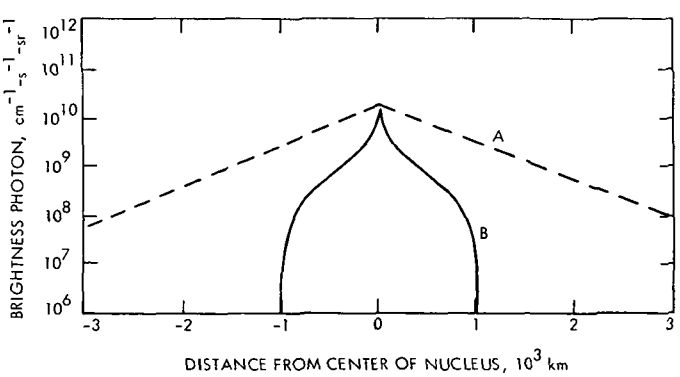

Fig. 30. Computed brightness profile in the visible continuum for Encke at a heliocentric distance of 1 AU assuming that the particulate component of the emission from the nucleus is (A) all dust and (B) all icy grains

(Ref. 16) where σ_0 is the initial area, and R_H is the radius of extent of the icy halo. For both ice and dust, an inverse square law is assumed for the number densities. The integration along the line of sight is similar to that described in Section IV-C.

The curves are normalized to a peak intensity of 20% of the intensity in the C_2 band to correspond to Liller's (Ref. 33) estimation of the relative intensities, corrected for the different bandwidths (see Section III-E-8). The actual curve for Encke probably has a shape somewhere between the two shown.

F. Secular Changes in the Visual Brightness of Encke

The absolute brightness of Encke has decreased steadily during the last century, and it is generally agreed that the comet will become completely inactive by around 2000 AD. Three groups of authors have studied the secular decay of Encke quantitatively. Whipple and Douglas-

Table 12. Photometric model for distances greater than 100,000 km from nucleus (outside coma)

R	********** THETA(DEGREES) **********				SURFACE BRIGHTNESS
KM.	D=10(5)KM.	D=10(6)KM.	D=10(7)KM.	D=10(8)KM.	PHOTONS CM-2 S-1 SR-1
12.5	.71620-02	.71620-03	.71620-04	.71620-05	.158860+12
15.6	.89525-02	.89525-03	.89525-04	.89525-05	.127084+12
19.5	.11191-01	.11191-02	.11191-03	.11191-04	.101663+12
24.4	.13988-01	.13988-02	.13988-03	.13988-04	.813267+11
30.5	.17485-01	.17485-02	.17485-03	.17485-04	.650574+11
38.1	.21857-01	.21857-02	.21857-03	.21857-04	.520419+11
47.7	.27321-01	.27321-02	.27321-03	.27321-04	.416296+11
59.6	.34151-01	.34151-02	.34151-03	.34151-04	.332997+11
74.5	.42689-01	.42689-02	.42689-03	.42689-04	.266358+11
93.1	.53361-01	.53361-02	.53361-03	.53361-04	.213046+11
116.4	.66701-01	.66701-02	.66701-03	.66701-04	.170397+11
145.5	.83376-01	.83376-02	.83376-03	.83376-04	.136278+11
181.9	.10422+00	.10422-01	.10422-02	.10422-03	.108983+11
227.4	.13028+00	.13028-01	.13028-02	.13028-03	.871464+10
284.2	.16284+00	.16284-01	.16284-02	.16284-03	.696773+10
355.3	.20355+00	.20356-01	.20356-02	.20356-03	.557020+10
444.1	.25444+00	.25444-01	.25444-02	.25444-03	.445217+10
555.1	.31805+00	.31806-01	.31806-02	.31806-03	.355774+10
693.9	.39756+00	.39757-01	.39757-02	.39757-03	.284220+10
867.4	.49695+00	.49696-01	.49696-02	.49696-03	.226976+10
1084.2	.62118+00	.62120-01	.62120-02	.62120-03	.181179+10
1355.3	.77646+00	.77650-01	.77650-02	.77650-03	.144541+10
1694.1	.97054+00	.97063-01	.97063-02	.97063-03	.115230+10
2117.6	.12131+01	.12133+00	.12133-01	.12133-02	.917790+09
2647.0	.15163+01	.15166+00	.15166-01	.15166-02	.730164+09
3308.7	.18951+01	.18958+00	.18958-01	.18958-02	.580040+09
4135.9	.23684+01	.23697+00	.23697-01	.23697-02	.459909+09
5169.9	.29595+01	.29621+00	.29621-01	.29621-02	.363766+09
6462.3	.36975+01	.37026+00	.37027-01	.37027-02	.286803+09
8077.9	.46183+01	.46282+00	.46283-01	.46283-02	.225172+09
10097.4	.57659+01	.57852+00	.57854-01	.57854-02	.175789+09
12621.8	.71937+01	.72314+00	.72317-01	.72318-02	.136184+09
15777.2	.89658+01	.90389+00	.90397-01	.90397-02	.104374+09
19721.5	.11156+02	.11298+01	.11300+00	.11300-01	.787677+08
24651.9	.13848+02	.14122+01	.14124+00	.14125-01	.580817+08
30814.9	.17127+02	.17650+01	.17656+00	.17656-01	.412843+08
38518.6	.21066+02	.22059+01	.22069+00	.22070-01	.275562+08
48148.2	.25710+02	.27566+01	.27587+00	.27587-01	.162976+08
60185.3	.31042+02	.34442+01	.34483+00	.34484-01	.727769+07
75231.6	.36955+02	.43024+01	.43104+00	.43105-01	.126604+07
94039.5	.43241+02	.53723+01	.53879+00	.53881-01	.296959+01

Table 13. Photometric model viewing toward nucleus for distances less than 100,000 km (inside coma)

R	***D=10(2)KM.***		***D=10(3)KM.***		***D=10(4)KM.***	
KM.	THETA(DEG)	BRIGHTNESS	THETA(DEG)	BRIGHTNESS	THETA(DEG)	BRIGHTNESS
12.5	.71250+01	.15640+12	.71616+00	.15884+12	.71620-01	.15886+12
15.6	.88807+01	.12402+12	.89517+00	.12705+12	.89525-01	.12708+12
19.5	.11051+02	.97864+11	.11189+01	.10163+12	.11191+00	.10166+12
24.4	.13720+02	.76626+11	.13985+01	.81279+11	.13988+00	.81326+11
30.5	.16971+02	.59272+11	.17480+01	.64998+11	.17485+00	.65057+11
38.1	.20880+02	.44977+11	.21846+01	.51968+11	.21857+00	.52041+11
47.7	.25494+02	.33098+11	.27300+01	.41537+11	.27321+00	.41629+11
59.6	.30797+02	.23150+11	.34111+01	.33184+11	.34151+00	.33299+11
74.5	.36688+02	.14790+11	.42610+01	.26491+11	.42688+00	.26635+11
93.1	.42963+02	.77879+10	.53207+01	.21124+11	.53359+00	.21303+11
116.4	.00000	.00000	.66402+01	.16815+11	.66698+00	.17038+11
145.5	.00000	.00000	.82795+01	.13347+11	.83371+00	.13625+11
181.9	.00000	.00000	.10309+02	.10550+11	.10421+01	.10895+11
227.4	.00000	.00000	.12810+02	.82830+10	.13025+01	.87110+10
284.2	.00000	.00000	.15866+02	.64354+10	.16280+01	.69632+10
355.3	.00000	.00000	.19559+02	.49181+10	.20347+01	.55645+10
444.1	.00000	.00000	.23946+02	.36613+10	.25428+01	.44450+10
555.1	.00000	.00000	.29035+02	.26114+10	.31773+01	.35488+10
693.9	.00000	.00000	.34756+02	.17294+10	.39693+01	.28311+10
867.4	.00000	.00000	.40937+02	.98794+09	.49572+01	.22559+10
1084.2	.00000	.00000	.00000	.00000	.61879+01	.17945+10
1355.3	.00000	.00000	.00000	.00000	.77130+01	.14238+10
1694.1	.00000	.00000	.00000	.00000	.96150+01	.11254+10
2117.6	.00000	.00000	.00000	.00000	.11956+02	.88441+09
2647.0	.00000	.00000	.00000	.00000	.14826+02	.68888+09
3308.7	.00000	.00000	.00000	.00000	.18308+02	.52926+09
4135.9	.00000	.00000	.00000	.00000	.22470+02	.39792+09
5169.9	.00000	.00000	.00000	.00000	.27338+02	.28887+09
6462.3	.00000	.00000	.00000	.00000	.32872+02	.19746+09
8077.9	.00000	.00000	.00000	.00000	.38931+02	.11992+09
10097.4	.00000	.00000	.00000	.00000	.00000	.00000
12621.8	.00000	.00000	.00000	.00000	.00000	.00000
15777.2	.00000	.00000	.00000	.00000	.00000	.00000
19721.5	.00000	.00000	.00000	.00000	.00000	.00000
24651.9	.00000	.00000	.00000	.00000	.00000	.00000
30814.9	.00000	.00000	.00000	.00000	.00000	.00000
38518.6	.00000	.00000	.00000	.00000	.00000	.00000
48148.2	.00000	.00000	.00000	.00000	.00000	.00000
60185.3	.00000	.00000	.00000	.00000	.00000	.00000
75231.6	.00000	.00000	.00000	.00000	.00000	.00000
94039.5	.00000	.00000	.00000	.00000	.00000	.00000

Hamilton (Ref. 11) fitted the observations for the period 1820–1955 to a law of the form

$$B = B(t_0)\,(1 - \lambda t)^2 \qquad (22)$$

in which constants $B(t_0)$ and λ are determined by a least squares fit. They obtained a value for the "death date" $t_d = 1/\lambda$ of 2000 AD (Fig. 5). Figure 6 shows observations of the brightness of Encke as presented by two Russian authors (Ref. 12). Sekanina (Ref. 31), in a detailed analysis of Marsden's (Ref. 50) data on the non-gravitational forces acting on Encke, has deduced a "death date" for this activity of 2030 AD. This date should coincide with the termination of visual activity, since both have the same origin, and is in quite good agreement with Whipple and Douglas-Hamilton's result.

The mean rate of decrease in the brightness of Encke in the last hundred years has been 3 magnitudes per century or 0.1 magnitude per revolution. Assuming that linear extrapolation is valid for the near future, an absolute visual magnitude of 11.1 is predicted for the 1980

Table 14. Photometric model viewing away from nucleus for distances less than 100,000 km (inside coma)

R	***D=10(2)KM.***		***D=10(3)KM.***		***D=10(4)KM.***	
KM.	THETA(DEG)	BRIGHTNESS	THETA(DEG)	BRIGHTNESS	THETA(DEG)	BRIGHTNESS
12.5	.17282+03	.24584+10	.17928+03	.24329+08	.17993+03	.20094+06
15.6	.17101+03	.30598+10	.17910+03	.30410+08	.17991+03	.25117+06
19.5	.16874+03	.37994+10	.17888+03	.38010+08	.17989+03	.31396+06
24.4	.16587+03	.47010+10	.17860+03	.47507+08	.17986+03	.39245+06
30.5	.16223+03	.57855+10	.17825+03	.59374+08	.17983+03	.49057+06
38.1	.15758+03	.70648+10	.17781+03	.74199+08	.17978+03	.61321+06
47.7	.15152+03	.85319+10	.17727+03	.92711+08	.17973+03	.76650+06
59.6	.14341+03	.10150+11	.17658+03	.11582+09	.17966+03	.95813+06
74.5	.13184+03	.11846+11	.17573+03	.14463+09	.17957+03	.11976+07
93.1	.11136+03	.13517+11	.17466+03	.18051+09	.17947+03	.14970+07
116.4	.00000	.00000	.17331+03	.22510+09	.17933+03	.18713+07
145.5	.00000	.00000	.17163+03	.28033+09	.17917+03	.23390+07
181.9	.00000	.00000	.16952+03	.34840+09	.17896+03	.29236+07
227.4	.00000	.00000	.16686+03	.43168+09	.17870+03	.36542+07
284.2	.00000	.00000	.16349+03	.53237+09	.17837+03	.45671+07
355.3	.00000	.00000	.15919+03	.65205+09	.17796+03	.57077+07
444.1	.00000	.00000	.15363+03	.79083+09	.17745+03	.71324+07
555.1	.00000	.00000	.14628+03	.94631+09	.17682+03	.89110+07
693.9	.00000	.00000	.13606+03	.11128+10	.17602+03	.11130+08
867.4	.00000	.00000	.11985+03	.12818+10	.17502+03	.13896+08
1084.2	.00000	.00000	.00000	.00000	.17378+03	.17337+08
1355.3	.00000	.00000	.00000	.00000	.17221+03	.21608+08
1694.1	.00000	.00000	.00000	.00000	.17025+03	.26888+08
2117.6	.00000	.00000	.00000	.00000	.16777+03	.33377+08
2647.0	.00000	.00000	.00000	.00000	.16465+03	.41280+08
3308.7	.00000	.00000	.00000	.00000	.16068+03	.50781+08
4135.9	.00000	.00000	.00000	.00000	.15557+03	.61990+08
5169.9	.00000	.00000	.00000	.00000	.14887+03	.74895+08
6462.3	.00000	.00000	.00000	.00000	.13974+03	.89342+08
8077.9	.00000	.00000	.00000	.00000	.12612+03	.10525+09
10097.4	.00000	.00000	.00000	.00000	.00000	.00000
12621.8	.00000	.00000	.00000	.00000	.00000	.00000
15777.2	.00000	.00000	.00000	.00000	.00000	.00000
19721.5	.00000	.00000	.00000	.00000	.00000	.00000
24651.9	.00000	.00000	.00000	.00000	.00000	.00000
30814.9	.00000	.00000	.00000	.00000	.00000	.00000
38518.6	.00000	.00000	.00000	.00000	.00000	.00000
48148.2	.00000	.00000	.00000	.00000	.00000	.00000
60185.3	.00000	.00000	.00000	.00000	.00000	.00000
75231.6	.00000	.00000	.00000	.00000	.00000	.00000
94039.5	.00000	.00000	.00000	.00000	.00000	.00000

apparition. This value is based on the most recent estimates* and is considerably brighter than Whipple and Douglas–Hamilton's law would predict. It should be regarded as uncertain by approximately 1 magnitude.

*IAU Circular No. 2547, and Z. Sekanina, private communication.

V. Optical Depth of the Coma

The optical thickness of the coma as a function of distance from the nucleus is an important quantity since it determines the evaporation rate of the nucleus and halo and determines the visibility of the nucleus. The fact that stellar condensations have been observed at the

Table 15. List of the strongest cometary emission bands at near-visible wavelengths

Band	Central wavelength, Å	Relative intensity (C_2 (0–0) = 1.0)
OH	3090	0.05
NH	3365	0.2
OH^+	3616[a]	0.01
CN (0–0)	3883	0.8
N_2^+	3914[b]	0.3
C_3	4050	0.4
CN (0–1)	4216	0.05
CH^+	4239[a]	0.01
CH	4281	0.07
C_2 (2–0)	4383	0.01
CO^+	4544[b]	0.9
C_2 (1–0)	4737	0.5
C_2 (0–0)	5165	1.0
NH_2 (0, 11, 0)	5600	0.5
C_2 (0–1)	5634	
NH_2 (0, 10, 0)	5700	0.05
C_2 (0–2)	6187	0.2
NH_2 (0, 9, 0)	6200	
NH_2 (0, 8, 0)	6300	0.1
NH_2 (0,7,0)	6600	0.05

[a]Observed in some comets but not yet in Encke.

[b]Principally found in the tail.

center of the head of many comets including Encke does not necessarily mean that the nucleus itself is observed; at ground-based resolution this object is just as likely to be the icy halo. For distances of more than a few hundred kilometers from the nucleus, stars are frequently observed through the coma without appreciable loss of brightness. At 600 km from the nucleus of Burnham, however, Dossin (Ref. 51) observed a stellar dimming of 1 magnitude, corresponding to an optical depth of 0.9. This implies (1) that the distribution of solid material may be highly asymmetric, and (2) that very active comets, at least, may be optically dense near the nucleus. The second conclusion is supported by Becklin and Westphal's observations of Ikeya–Seki at infrared wavelengths (Ref. 52). The 10-μm brightness they measured, extrapolated to 1 AU, is equivalent to a 300 K black body with a radius of 10^3 km. This result implies that this comet had a very extensive optically thick halo.

The optical depth in the atmosphere of the Encke model is evaluated, assuming an extinction cross section for the grains and dust equal to the geometrical cross section. Then the optical thickness $d\tau$ of an elementary shell of thickness dr at a radial distance r from the center of the nucleus is

$$d\tau = \frac{\Sigma\, n\sigma}{4\pi r^2}\frac{dr}{v} \tag{23}$$

where n is the total number of particles of cross-section σ emitted per second, and v is the terminal velocity. So the optical depth down to the surface of the nucleus (of radius R_n) is

$$\tau = \int_{\infty}^{R_n} \frac{\sum \frac{n\sigma}{v}}{4\pi r^2}\, dr = \frac{1}{4\pi R_n}\sum \frac{n\sigma}{v} \tag{24}$$

For the icy halo alone, $n = 10^{10}$ s^{-1} (Section III-D-2), $\sigma = 10^{-3}$ cm^2 (Section III-D-1), and $v = 10^3$ cm-s^{-1} (Fig. 19). Using $R_n = 1.3$ km, we find $\tau \simeq 10^{-2}$. The contribution of the particles in the dust model is somewhat smaller than this, so the conclusion is that only about 1% of the continuum radiation reaching the nucleus is lost. This result is uncertain by perhaps 2 orders of magnitude, corresponding to upper and lower limits on the optical thickness of Encke's atmosphere of 1 and 10^{-4}, respectively.

VI. Temperature Variation of the Nucleus With Heliocentric Distance

Two extremes can be considered. If the nucleus is covered with ices, then its temperature is controlled by the latent heat of vaporization of the condensate. Delsemme (Ref. 23) has studied this problem and concludes that the temperature of the nucleus should reach 200 K at about 4 AU and remain fairly constant until perihelion. If, on the other hand, the nucleus is mostly depleted of ice on its surface, then the asteroidal law (Ref. 53)

$$T = \frac{350}{\Delta^2} \tag{25}$$

should be followed. This latter case probably applies fairly closely to Encke after perihelion when most surface condensates have been boiled off. During its approach to the Sun, the dependence probably lies between the two extremes. Figure 31 shows a plot of the situation for 10% of the surface occupied by ice-containing pores.

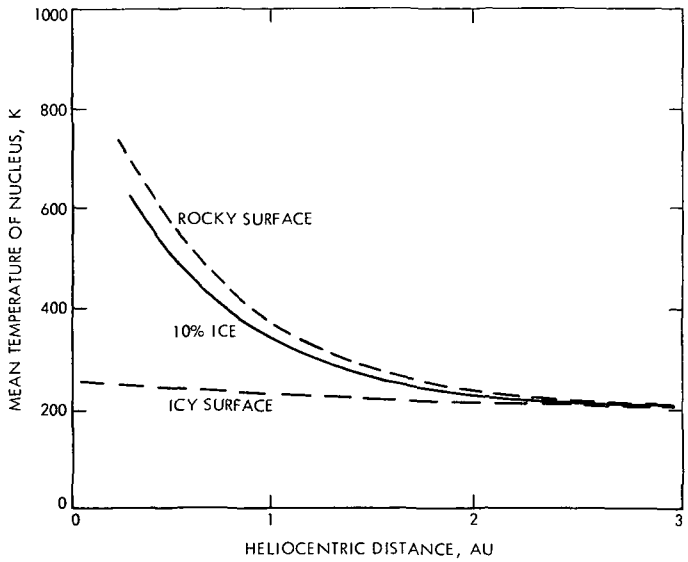

Fig. 31. Mean temperature of the nucleus as a function of distance from the Sun and surface composition

References

1. Whipple, F. L., and Hamid, S. E., *Bull. Roy. Obs. Helwan*, No. 41, p. 30, 1952.
2. Roemer, E., "Comet Notes," *Mercury*, Vol. I, No. 6, pp. 18–19, 1972.
3. Vsekhsvyatskii, S. K., *Physical Characteristics of Comets*, NASA TT F-80, Office of Technical Services OTS 62-11031, National Aeronautics and Space Administration, Washington, D. C., 1964.
4. Roemer, E., "The Dimensions of Cometary Nuclei," *Mem. Soc. Roy. des Sci. de Liège*, Vol. 12, p. 23, 1966.
5. Matson, D. L., "Infrared Observations of Asteroids," in *Physical Studies of Minor Planets*, Proceedings of the 12th IAU Colloquium, NASA SP-267, p. 45, edited by T. Gehrels, National Aeronautics and Space Administration, Washington, D. C., 1971.
6. Marsden, B. G., and Sekanina, Z., quoted in Ref. 9.
7. Maines, P., Grudinska, S., and Stawiskowski, A., "Observations Physiques de la Comète Périodique Giacobini-Zinner (1959b)," *Annales d'Astrophysique*, Vol. 23, pp. 788–796, 1950.
8. Yeomans, D. K., *Physical Description and Recovery Data for P/Encke*, unpublished report, Computer Sciences Corp., Silver Springs, Md., Apr. 1973.

References (contd)

9. *Study of a Comet Rendezvous Mission,* Technical Report No. 72-87, TRW Systems Group, Redondo Beach, Calif., May 1972.

10. Whipple, F. L., "A Comet Model. 1. The Acceleration of Comet Encke," *Astrophys. J.,* Vol. 111, pp. 375–394, 1950.

11. Whipple, F. L., and Douglas-Hamilton, D. H., "Brightness Changes in Periodic Comets," *Mem. Soc. Roy. des Sci. de Liège,* Vol. 12, pp. 469–480, 1965.

12. Vsekhsvyatskii, S. K., and Illichishina, N. I., "Absolute Magnitudes of Comets, 1965–1969," *Sov. Astron.,* Vol. 15, p. 310, 1971.

13. Sekanina, Z., "A Model for the Nucleus of Encke's Comet," IAU Symposium No. 45, pp. 301–307, edited by G. A. Chebotarev, E. I. Kazimirchak-Polonskaya, and B. G. Marsden, Springer-Verlag, Inc., New York, 1972.

14. Delsemme, A. H., and Wenger, A., "Physico-Chemical Phenomena in Comets —I. Experimental Studies of Snows in a Cometary Environment," *Planet. Space Sci.,* Vol. 18, p. 709, 1970.

15. Delsemme, A. H., and Miller, D. C., "Physico-Chemical Phenomena in Comets —II. Gas Adsorption in the Snows of the Nucleus," *Planet. Space Sci.,* Vol. 18, p. 717, 1970.

16. Delsemme, A. H., and Miller, D. C., "Physico-Chemical Phenomena in Comets —III. The Continuum of Comet Burnham (1960 II)," *Planet. Space Sci.,* Vol. 19, p. 1229, 1971.

17. Delsemme, A. H., and Miller, D. C., "Physico-Chemical Phenomena in Comets —IV. The C_2 Emission of Comet Burnham (1960 II)," *Planet. Space Sci.,* Vol. 19, p. 1259, 1971.

18. Opik, E. J., "The Stray Bodies in the Solar System, Part II. The Cometary Origin of Meteorites," *Advan. Astron. Astrophys.,* Vol. 4, p. 302, 1966.

19. Whipple, F. L., *Proc. Amer. Phil. Soc.,* Vol. 83, p. 711, 1940.

20. Goldberg, R. A., and Aikin, A. C., "Comet Encke: Meteor Metallic Ion Identification by Mass Spectrometer," *Science,* Vol. 180, pp. 294–296, 1973.

21. Jacchia, L. G., "Meteors, Meteorites and Comets: Interrelations," in *The Moon, Meteorites and Comets,* edited by B. M. Middlehurst and G. P. Kuiper, University of Chicago Press, Chicago, Ill., 1963.

22. Wood, J. A., "Physics and Chemistry of Meteorites," in *The Moon, Meteorites and Comets,* edited by B. M. Middlehurst and G. P. Kuiper, University of Chicago Press, Chicago, Ill., 1963.

23. Delsemme, A. H., "Vers un Modelle Physico-Chemique du Noyeau Cometaire," *Mem. Soc. Roy. des Sci. de Liège,* Vol. 12, p. 77, 1966.

24. Jackson, W. M., and Donn, B., "Collisional Processes in the Inner Coma," *Mem. Soc. Roy. des Sci. de Liège,* Vol. 12, p. 133, 1965.

25. Wurm, K., and Mannano, A., "Dissoziation and Ionization in Kometen," *Icarus,* Vol. 6, p. 281, 1967.

References (contd)

26. Wurm, K., "Structure and Kinematics of Cometary Type I Tails," *Icarus*, Vol. 8, p. 287, 1968.

27. Rahe, J., "The Structure of Tail Rays in the Coma Region of Comets," *Z. Astrophys.*, Vol. 68, p. 208, 1968.

28. Rahe, J., and Donn, B., "Ionization and Ray Formation in Comets," *Astron. J.*, Vol. 74, p. 256, 1969.

29. Bertaux, J. L., Blamont, J. E., and Festou, M., "Interpretation of Hydrogen Lyman-α Observations of Comets Bennett and Encke," *Astron. Astrophys.* (in press).

30. Delsemme, A. H., "Cometary Nuclei," in *Extraterrestrial Matter*, p. 304, edited by C. A. Randall, Northern Illinois University Press, DeKalb, Ill., 1969.

31. Sekanina, Z., "Dynamical and Evolutionary Aspects of Gradual Deactivation of Short-Period Comets," *Astron. J.*, Vol. 74, No. 10, p. 1223, 1970.

32. Mendis, D. A., Holzer, T. E., and Axford, W. I., "Neutral Hydrogen in Cometary Comas," *Astrophys. Space Sci.*, Vol. 15, p. 313, 1972.

33. Liller, W., "Photoelectric Photometry of Comets," *Astron. J.*, Vol. 66, No. 8, p. 372, 1961.

34. Finson, M. J., and Probstein, R. F., "A Theory of Dust Comets. I. Model and Equations," *Astrophys. J.*, Vol. 154, No. 1, Part 1, p. 327, 1968.

35. Lovell, A. C. B., *Meteor Astronomy*, Oxford University Press, London, 1954.

36. Millman, P. M., and McKinley, D. W. R., "Meteors," in *The Moon, Meteorites and Comets*, edited by B. M. Middlehurst and G. P. Kuiper, University of Chicago Press, Chicago, Ill., 1963.

37. McCrosky, R., *Orbits of Photographic Meteors*, Special Report 257, Smithsonian Institution Astrophysical Observatory, Cambridge, Mass., 1967.

38. Finson, M. J., and Probstein, R. F., "A Theory of Dust Comets. II. Results for Comet Arend-Roland," *Astrophys. J.*, Vol. 154, No. 1, Part 1, p. 353, 1968.

39. Sekanina, Z., and Miller, P. D., "Comet Bennett 1970 II," *Science*, Vol. 179, pp. 565–567, 1973.

40. Sekanina, Z., "Total Gas Concentration in Atmospheres of the Short Period Comets and Impulsive Forces Upon Their Nuclei," *Astron. J.*, Vol. 74, pp. 944–950, 1969.

41. Probstein, R. F., *Problems of Hydrodynamics and Continuum Mechanics*, p. 568, Society for Industrial and Applied Mechanics, Philadelphia, Pa., 1968.

42. Richter, N., *Monatsber. Deut. Akad. Wiss. Berlin*, Vol. 1, p. 727, 1959.

43. Peterson, J. T., and Weinman, J. A., "Optical Properties of Dust Particles at Infrared Wavelengths," *J. Geophys. Res.*, Vol. 74, p. 6947, 1969.

44. Spitzer, W. G., and Kleinman, D. A., "Infrared Lattice Bands of Quartz," *Phys. Rev.*, Vol. 121, p. 1324, 1961.

References (contd)

45. Sauer, C. G., *Encounter Parameters for Encke Slow Flyby Mission,* unpublished.

46. Roemer, E., "Comets: Discovery, Orbits, Astrometric Observations," in *The Moon, Meteorites and Comets,* edited by B. M. Middlehurst and G. P. Kuiper, University of Chicago Press, Chicago, Ill., 1963.

47. Wurm, K., "The Physics of Comets," in *The Moon, Meteorites and Comets,* edited by B. M. Middlehurst and G. P. Kuiper, University of Chicago Press, Chicago, Ill., 1963.

48. Swings, P., and Haser, L., *Atlas of Representative Cometary Spectra,* Technical Report, University of Liège Astrophysical Institute, Liège, France, 1955.

49. O'Dell, C. R., "Emission-Band and Continuum Photometry of Comet Burnham, 1959k," *Publ. Astron. Soc. Pacific,* Vol. 73, p. 35, 1961.

50. Mardsen, B. G., "Comets and Non-Gravitational Forces III," *Astron. J.,* Vol. 75, p. 75, 1970.

51. Dossin; F., "Observation of the Diminution of Star Brightness Seen Through the Central Region of Burnham's Comet (1959k)," *J. Obsrs.,* Vol. 45, p. 1, 1962.

52. Becklin, E. E., and Westphal, J. A., "Infrared Observations of Comet 1965f," *Astrophys. J.,* Vol. 145, pp. 445–453, 1966.

53. Levin, B. J., "Are Gases Evaporated or Desorbed from Cometary Nuclei?" *Mem. Soc. Roy. des Sci. de Liège,* Vol. 12, p. 65, 1966.

NASA — JPL — Coml., L.A., Calif.